

Parity-violating quasifree electron-deuteron scattering in a covariant approach.

Grigorios I. Poulis

*Department of Physics and Mathematical Physics
and Special Research Center for the Subatomic Structure of Matter
University of Adelaide, SA 5005, Australia
(Report #: ADP-96-47/T241, to appear in *Few Body Systems*)*

The role of relativistic corrections associated with lower Dirac components of the deuteron wavefunction, is examined for parity-violating (PV) electron scattering. The relation between these corrections and negative energy components of the struck nucleon in relativistic PWIA is elucidated. The model dependence induced by describing such effects, using different deuteron vertex functions and prescriptions for the half-off-shell nucleon vertices, is compared against the precision required for studies of nucleon strangeness in quasielastic PV $e-d$ scattering.

I. MOTIVATION

Measuring the parity-violating (PV) longitudinal asymmetry in electron scattering offers the possibility to extract the hitherto unknown vector, $G_{E,M}^s$, and (though to much less extent) axial vector, G_A^s , strangeness nucleon form factors. Several such measurements will be performed in medium energy facilities, such as MIT-Bates [1], Mainz-MAMI [2] and TJNAF [3]. The first phase of the SAMPLE experiment [4] at MIT-Bates is currently under way and will attempt to extract G_M^s from low momentum transfer, $q^2 = -0.1$ (GeV/c)², backward angle, elastic PV $e-p$ scattering. However, strong correlation with the neutral current (NC), axial, isovector form factor, $\tilde{G}_A^{T=1}$, whose radiative corrections have a large theoretical uncertainty in the Standard Model [5], places constraints on the effectiveness of the SAMPLE measurement. Hadjimichael et al. suggested [6] that a complimentary measurement of the PV asymmetry in quasielastic scattering from deuterium, may, in conjunction with the proton measurement, allow one to determine both G_M^s and $\tilde{G}_A^{T=1}$. The rationale of this suggestion is that, although both G_M^s and $\tilde{G}_A^{T=1}$ appear in the (predominantly transverse) backward asymmetry multiplied by magnetic ($G_M^{p,n}$) form factors, they come with different weighting for a nuclear target, i.e., $(ZG_M^p + NG_M^n)$ vs. $(ZG_M^p - NG_M^n)$, being, respectively, isoscalar and isovector. Thus, for deuterium, this correlation is suppressed relatively to the proton by approximately $(\mu_p - \mu_n)/(\mu_p + \mu_n) > 5$. Following this analysis, SAMPLE (in its second phase) as well as the E91-017 experiment at TJNAF [3], and

possibly a future experiment at Mainz [2] will perform such measurements on deuterium.

In attempting to extract such subtle subnuclear effects from a *nuclear* observable, it is imperative that the nuclear physics modeling can be trusted to the 1-2% level. In Ref. [6] the theoretical uncertainty was estimated for the deuteron case, and was concluded that relativistic, rather than rescattering effects, are the main source of model dependence in the PV asymmetry for quasifree kinematics at $|\mathbf{q}| > 0.7$ GeV/c, especially at forward angles (6% effects). This follows from a comparison of a traditional potential calculation including final-state interactions (FSI), where the current operators were truncated to first nontrivial order in a nonrelativistic expansion, with a plane wave impulse approximation (PWIA) calculation, in which a nonrelativistic momentum distribution is convoluted with a relativistic off-shell single nucleon tensor obtained by a generalization of de Forest's "cc" prescriptions [8] to be used with the weak neutral current. At low momentum transfer, where relativistic corrections are –presumably– not important, the FSI calculation should be used [7]. At TJNAF energies, though, the nonrelativistic expansions in the FSI calculation are inadequate, while, on the other hand, rescattering effects are expected to be suppressed — and therefore the PWIA calculation should be preferred. In adopting this point of view, the 6% effects at $|\mathbf{q}| > 0.7$ GeV/c, which, if taken at face value threaten the interpretability of PV deuterium measurements, are not viewed as a fair measure of nuclear uncertainty; rather, the FSI model should be considered not applicable for such kinematics [9].

The PWIA calculation, however, is a semirelativistic, rather than a covariant calculation, in that it treats the deuteron as a nonrelativistic bound state. On the other hand, much work has been devoted to relativistic treatments of $e-d$ scattering, in the sense of consistent nonrelativistic expansions including wave function and boost effects [10], as well as covariant solutions of the bound state using the Bethe-Salpeter equation [11–13] or its "spectator" version [14,15]. Given the availability of such relativistic treatments, and the degree of precision required for strangeness studies, the basic objective of this work is to calculate the PV $e-d$ asymmetry in a covariant model. In doing so, our motivation is different

from most studies of relativistic effects, where observables exhibiting large such effects are sought after, in the hope to probe details of nuclear dynamics. In our case we wish to be as independent as possible from nuclear dynamics. We wish to quantify that the *residual* relativistic effects which are associated with a relativistically described deuteron bound state, and are, therefore, *not* included in the semirelativistic PWIA, are small and, for the PV asymmetry, less than 1% for the kinematics of interest. Since the high-momentum bound nucleons are suppressed due to Fermi motion, it is reasonable to expect such residual relativistic effects to be small. Establishing such a result is important for high q^2 quasifree experiments at TJNAF with heavier nuclei as targets, for which a semirelativistic PWIA is possible but a covariant calculation is not (notwithstanding the fact that the effects reported here for the deuteron will underestimate those for such heavier nuclei due to the uncharacteristically loose binding ($k_F \approx 60$ MeV/c) of the deuteron).

Although ultimately we would like to have a covariant formulation of PV $e - d$ scattering following the more fundamental approach of Hummel and Tjon [12], a simpler approach is taken here, following that of Keister and Tjon [11] and Beck et al. [16]. It amounts to a covariant, or “relativistic” (R) PWIA. Unlike the semirelativistic, or factorized (F) PWIA, in which the deuteron is treated nonrelativistically, in this case the hadronic tensor does not factorize in the strong sense, i.e., cannot be written as a convolution of a single-nucleon tensor with a momentum distribution. This is due to the off-shellness of the propagating nucleon. By separating the forward (positive energy) and backward (negative energy) components of the struck nucleon’s propagator, we find a “weak” form of factorization, where the momentum distribution and the single-nucleon tensor become density matrices. As a byproduct of this construction, we can identify the *ad hoc* prescription in the factorized (F) PWIA of de Forest, simply, as a projection of the covariant hadronic tensor of the RPWIA onto the positive energy sector, which shows the relation between off-shell and relativistic effects. Since it is off-shell effects that spoil factorization in RPWIA, we expect, and indeed observe numerically, that the effects of the projection are minimal on the quasielastic peak, where kinematics are “maximally on-shell”.

The structure of this article is as follows. In Sect. II we discuss the relativistic calculation (RPWIA) used in this work. In Sect. III we review the factorized PWIA, and discuss the projection by which the FPWIA is obtained from RPWIA. In Sect. IV we show numerical results for the cross section and the PV asymmetry for the kinematics of interest, and discuss the role of the residual relativistic effects in the interpretation of experiments designed to study nucleon

strangeness. Our conclusions appear in Sect. V and some details of the calculation in the Appendices.

II. THE HADRONIC TENSOR IN RELATIVISTIC PWIA

The kinematics for deuteron electrodisintegration, in PWIA and in the target rest frame, $d^\mu = (M_d, \mathbf{0})$, are shown in Fig. 1(a). The momentum transfer is $q^\mu = (\omega, \mathbf{q})$, and, for the moment, we assume that the nucleon $p^\mu = (E_p, \mathbf{p})$ is detected in coincidence with the electron $e'^\mu = (\epsilon', \mathbf{u}')$, while the other nucleon $n^\mu = (E_n, -\mathbf{k})$ is not. Here $d^2 = M_d^2$, $p^2 = n^2 = m^2$. The cross section is obtained from

$$d\sigma^{(h)} = \frac{\alpha^2 d\mathbf{u}' d\mathbf{p} d\mathbf{n}}{q^4 (2\pi)^3 M_d} \frac{m_e^2}{\epsilon \epsilon'} \frac{m^2}{E_p E_n} \delta^4(P_f - P_i) l_{\mu\nu} H^{\mu\nu}, \quad (1)$$

where $P_i^\mu = d^\mu + q^\mu$, $P_f^\mu = p^\mu + n^\mu$, $l_{\mu\nu}$ is the leptonic,

$$l_{\mu\nu} = \sum_{h'} \langle e', h' | \gamma_\mu | e, h \rangle^* \langle e', h' | \gamma_\nu | e, h \rangle, \quad (2)$$

and $H^{\mu\nu}$ the hadronic tensor

$$H^{\mu\nu} = \overline{\sum}_{\text{spins}} \langle f | \hat{J}_p^\mu | i \rangle^* \langle f | \hat{J}_p^\nu | i \rangle, \quad (3)$$

and where spin d.o.f. have been averaged over in the unpolarized target ($|i\rangle = |d\rangle$) state and summed over in the final electron and np states. The plane-wave impulse approximation (PWIA) amounts to (I) using one-body current operators J^μ , (II) disregarding final-state interactions, and (III) assuming that the detected nucleon is identified with the (off-shell, $k^2 < m^2$) nucleon $k^\mu = (E_k, \mathbf{k})$ struck by the virtual boson [8,17]. Under these assumptions the PWIA amplitude reduces to that of Fig. 1(b). The inclusive cross section in PWIA with polarized electron beam and unpolarized target is obtained by integrating over $d^3\mathbf{n}$ and $d\Omega_k$ using the energy-momentum δ -function [18]

$$\begin{aligned} \frac{d^2\sigma^{(h)}}{d\Omega_e dw} &= \frac{1}{(2\pi)^2} \frac{1}{M_d} \sigma_M \int_{|y|}^Y d|\mathbf{k}| |\mathbf{k}| \frac{m^2}{q\sqrt{m^2 + |\mathbf{k}|^2}} \\ &\times \sum_{i=p,n} (v_L W_L^i + v_T W_T^i + h v_{T'} W_{T'}^i) \quad (4) \\ &\equiv \sigma_M \left[v_L R^L + v_T R^T + h v_{T'} R^{T'} \right]. \end{aligned}$$

Here σ_M is the Mott cross section. The limits of integration, $|y|$ and Y , as well as the responses R are

functions of $|\mathbf{q}|$ and ω .¹ The lepton kinematics are included in the factors [19]

$$v_L = \left[\frac{q^2}{\mathbf{q}^2} \right]^2, \quad v_T = \frac{1}{2} \left| \frac{q^2}{\mathbf{q}^2} \right| + \tan^2 \frac{\theta}{2}$$

$$v_{T'} = \tan \frac{\theta}{2} \sqrt{\left| \frac{q^2}{\mathbf{q}^2} \right| + \tan^2 \frac{\theta}{2}}. \quad (5)$$

The incoherent sum over nucleons in Eq. (4) is a consequence of assumption (III) above [17]. The responses W^i are obtained as components of the hadronic tensor in Eq. (3).

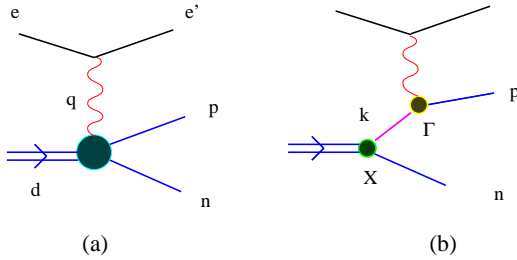


FIG. 1. Deuteron electrodisintegration in PWIA.

In relativistic (R) PWIA the hadronic tensor is obtained from the amplitude in Fig. 1(b)

$$\langle f | \hat{J}^\mu | i \rangle \sim \bar{u}(p) \Gamma^\mu \frac{\not{k} + m}{k^2 - m^2} \mathcal{X}_\nu \xi^\nu v(n). \quad (6)$$

Here Γ^μ is the half-off-shell nucleon vertex, ξ_ν is the deuteron polarization vector and \mathcal{X}^ν is the d-p-n vertex. Having applied charge conjugation to the on-shell nucleon $|n\rangle$, rather than the off-shell one $|k\rangle$, \mathcal{X}^μ is obtained from the Blankenbecler and Cook [20] vertex, \mathcal{V}^μ , according to

$$\mathcal{X}_\nu = C^T \mathcal{V}_\nu^T C^T$$

$$= A \gamma_\nu + \frac{B}{m} r_\nu + \frac{m - \not{k}}{2m} \left[F \gamma_\nu + \frac{G}{m} r_\nu \right], \quad (7)$$

with C the charge conjugation operator, and $r^\nu = (n^\nu - k^\nu)/2$. The vertex functions A, B, F, G depend on k^2 and can be written in terms of the ${}^3S_1(u)$, ${}^3D_1(w)$, ${}^3P_1(v_i)$ and ${}^1P_1(v_s)$ relativistic deuteron wavefunctions [11,14]. In the on-shell matrix element $\bar{u}(k) \mathcal{X}_\nu v(n)$ the off-shell F, G vertex functions would not contribute. Squaring the amplitude in Eq. (6),

¹ the T' response is included anticipating the discussion of parity-violation below; it is identically zero for purely electromagnetic (EM), inclusive, unpolarized target scattering.

summing over spins in the final state, and averaging over deuteron polarizations, one obtains for the hadronic tensor in RPWIA

$$H_{\text{RPWIA}}^{\mu\nu} = \frac{-g_{\rho\lambda} + d_\rho d_\lambda / M_d^2}{3(k^2 - m^2)^2} \text{Tr} \left\{ \frac{\not{k} - m}{2m} \bar{\mathcal{X}}^\rho (\not{k} + m) \right.$$

$$\left. \times \bar{\Gamma}^\mu \frac{\not{p} + m}{2m} \Gamma^\nu (\not{k} + m) \mathcal{X}^\lambda \right\}, \quad (8)$$

where $\bar{\mathcal{X}}_\nu = \gamma_0 \mathcal{X}_\nu^\dagger \gamma_0$ and similarly for $\bar{\Gamma}_\mu$. Following Keister and Tjon [11] we define auxiliary vectors \mathcal{P}^μ , S^μ and scalars β , T through

$$(\mathcal{P} + \beta) = (-g_{\rho\lambda} + d_\rho d_\lambda / M_d^2) \mathcal{X}^\lambda (\not{k} - m) \bar{\mathcal{X}}^\rho \quad (9)$$

$$(\mathcal{S} + T) = \frac{\not{k} + m}{2m} (\mathcal{P} + \beta) \frac{\not{k} + m}{2m}, \quad (10)$$

implying

$$(2m)^2 S^\mu = 2 [m\beta + (k \cdot \mathcal{P})] k^\mu + (m^2 - k^2) \mathcal{P}^\mu$$

$$(2m)^2 T = (k^2 + m^2) \beta + 2m(k \cdot \mathcal{P}). \quad (11)$$

We thus obtain

$$H_{\text{RPWIA}}^{\mu\nu} = \frac{4m^2}{3(k^2 - m^2)^2} \text{Tr} \left\{ \frac{\mathcal{S} + T}{2m} \bar{\Gamma}^\mu \frac{\not{p} + m}{2m} \Gamma^\nu \right\}. \quad (12)$$

Expressions for \mathcal{P} , β , and the hadronic tensor can be found in Appendix A. Equations (12) and (11) provide a reference point for a comparison with the factorized (F), or ‘‘semirelativistic’’, PWIA, that is widely used in intermediate energy physics.

III. REDUCTION OF RPWIA TO FPWIA

A. Factorized PWIA revisited

In FPWIA the cross section is written as a convolution of a nonrelativistic momentum distribution $\rho = \rho(|\mathbf{k}|)$ with a single nucleon cross section [8,18]

$$\frac{d^2 \sigma^{(h)}}{d\Omega_e dw} = 2\pi \sigma_M \int_{|y|}^Y d|\mathbf{k}| |\mathbf{k}| \rho(|\mathbf{k}|) \frac{m^2}{q\sqrt{m^2 + |\mathbf{k}|^2}}$$

$$\times \sum_{i=p,n} [v_L \mathcal{W}_L^i + v_T \mathcal{W}_T^i + h v_{T'} \mathcal{W}_{T'}^i], \quad (13)$$

The *single nucleon* responses $\mathcal{W}_{L,T,T'}$ are obtained as components of a covariant single nucleon tensor $\mathcal{H}^{\mu\nu}$, describing the interaction of a moving, off-shell nucleon with the virtual photon. The most general form of the off-shell vertex has been obtained by Bincer [21]. The special case of the half-off-shell vertex $\bar{u}(p) \Gamma^\mu$ involves four independent vertex functions of two scalar variables, e.g., q^2 and k^2 , and collapses

to the familiar form involving just two form factors (Dirac, F_1 , and Pauli, F_2) when operating on an on-shell spinor $u(k)$. The half-off-shell vertex functions of composite particles cannot be uniquely defined [22,23]. They can of course be computed in specific models [24,25], but then the whole reaction (i.e., the self energy and the d-p- \bar{n} vertex) should be, as well. Since such simple models are not realistic (i.e., they do not reproduce the observable on-shell form factors F_1 and F_2) it has become customary to resort to *ad hoc* prescriptions for treating the half-off-shell single nucleon tensor, the most widely used of which are the “cc” prescriptions of de Forest [8]. These prescriptions involve a set of operations regarding

- I. the wavefunction of the struck off-shell nucleon.
- II. the form of the half-off-shell vertex.
- III. the treatment of current conservation.

With respect to (I), the struck, off-shell nucleon wavefunction is taken to be that of the corresponding “would-be-on-shell” spinor $u(\bar{k})$, with same spatial momentum \mathbf{k} , but (positive) energy $\bar{E}_k = E_n = \sqrt{m^2 + \mathbf{k}^2} > E_k$. As we discuss in the next section, by reformulating (I) in a more transparent fashion, it is this approximation that differentiates between RPWIA and FPWIA.

With respect to (II) the following two vertices are employed

$$\begin{aligned} \Gamma_2^\mu &= F_1 \gamma^\mu + i \frac{q_\nu}{2m} \sigma^{\mu\nu} F_2 \\ &\hookrightarrow (F_1 + F_2) \gamma^\mu - \frac{(k+p)^\mu}{2m} F_2 + \gamma^\mu F_2 \frac{(\not{k}-m)}{2m} \\ \Gamma_1^\mu &= (F_1 + F_2) \gamma^\mu - \frac{(\bar{k}+p)^\mu}{2m} F_2, \end{aligned} \quad (14)$$

where the second equation in (14) is to be understood in the sense of the Gordon decomposition of $\bar{u}(p)\Gamma_2^\mu$. In the Γ_1^μ vertex appears the auxilliary four-vector $\bar{k}^\mu \equiv (\bar{E}_k, \mathbf{k})$, instead of $k^\mu = (E_k, \mathbf{k})$. In the on-shell case, the Gordon decomposition of $\bar{u}(p)\Gamma_2^\mu u(k)$ is complete and the Γ_1^μ , Γ_2^μ vertices matrix-element-equivalent. The difference between results obtained using the two forms of the vertex is interpreted as an estimate of the theoretical uncertainty induced in the modeling of the reaction because of our inability to calculate reliably the half-off-shell vertex functions from first principles [8,26]. Thus, under I and II, the single nucleon tensor reads

$$\mathcal{H}_{\text{FPWIA}}^{\mu\nu} = \text{Tr} \left(\frac{\bar{k}+m}{2m} \bar{\Gamma}_{1,2}^\mu \frac{\not{p}+m}{2m} \Gamma_{1,2}^\nu \right), \quad (15)$$

where (I) has resulted in the positive energy projector with the auxilliary four-vector \bar{k} .

With respect to III, one notices that, in the half-off-shell case, the one-body current is not conserved [24], since $q_\mu \bar{u}(p)\gamma^\mu = \bar{u}(p)(m - \not{k})$. The de Forest “cc” prescriptions enforce current conservation $\mathbf{J} \cdot \mathbf{q} = J_0\omega$ by eliminating the third component of the current in favor of the charge density, where \mathbf{q} defines the z-axis. Alternatively, one may choose to eliminate the charge in favor of J_3 , or not enforce current conservation at all. In Ref. [26] it was shown that the treatment of current conservation induces, especially in high missing momentum kinematics in $(e, e'p)$ processes, a substantial uncertainty. Recently, the three ways of treating current conservation have been shown to be equivalent to specific gauge choices within a family of covariant gauges [27]. Thus, the RPWIA approach described here is covariant, but not gauge invariant.

B. Strong vs. Weak Factorization

The question we address here is under which set of operations (related to assumption (I) above) is the FPWIA of Eqs. (13) and (15) obtained from the RPWIA of Eqs. (4) and (12)

$$H_{\text{RPWIA}}^{\mu\nu} \stackrel{?}{\rightarrow} (2\pi)^3 M_d \rho \mathcal{H}_{\text{FPWIA}}^{\mu\nu}. \quad (16)$$

We start by observing that from Eq. (11) one has

$$\mathcal{S}+T = 2 [m\beta + (k \cdot \mathcal{P})] \frac{\not{k}+m}{4m^2} + \frac{m^2 - k^2}{4m^2} [\mathcal{T} - \beta]. \quad (17)$$

Since \mathcal{P}^ν is obtained from the deuteron vertex functions [cf. Eq. (9)], the second term in Eq. (17) does not allow to factor all dependence on details of the deuteron break-up amplitude out of the trace of Eq. (12), thus defining a “single nucleon” tensor. However, if one ignores the off-shellness of the struck nucleon and sets $k^\mu \rightarrow \bar{k}^\mu$ in Eq. (11), one obtains

$$4m^2(\mathcal{S}+T) \rightarrow 2 [m\beta + (\bar{k} \cdot \mathcal{P})] (\bar{k} + m). \quad (18)$$

Comparison with Eqs. (4), (12), (13) and (15) shows that the cross section has indeed the factorized form of the “semirelativistic” FPWIA, provided that the nonrelativistic momentum distribution ρ is related to the quantity $[m\beta + (\bar{k} \cdot \mathcal{P})] / [12\pi^3 M_d (k^2 - m^2)^2]$. We shall return to this later on. The relevant observation at this point is that the RPWIA is *not* factorizable, unless the off-shellness of the struck nucleon is ignored.² To probe this issue further, we use the familiar technique of interpreting the propagation of the

² analogous observations can be made for the case of deep inelastic scattering processes [28].

off-shell struck nucleon as a superposition of positive and negative (on-shell) energy states (see, e.g., Ref. [29], or Arnold et al. [15], where a similar formalism is developed for elastic $e-d$ scattering)

$$\frac{\mathbf{k}+m}{2m} = f_+ \frac{\mathbf{k}_+ + m}{2m} + f_- \frac{\mathbf{k}_- - m}{2m}, \quad (19)$$

where

$$f_{\pm} = (E_k \pm \bar{E}_k)/2\bar{E}_k, \quad \text{and} \quad k_{\pm}^{\mu} = (\bar{E}_k, \pm \mathbf{k}). \quad (20)$$

The decomposition, Eq. (19), is frame-dependent. Notice, in particular, that in the deuteron rest frame the on-shell states are the struck and spectator nucleon, respectively, i.e., $k_+^{\mu} = \bar{k}^{\mu}$ and $k_-^{\mu} = n^{\mu}$. We now write Eq. (19) in terms of the direct products of these on-shell states

$$\frac{\mathbf{k}+m}{2m} = f_+ \sum_s u(\mathbf{k}, s) \bar{u}(\mathbf{k}, s) + f_- \sum_s v(-\mathbf{k}, s) \bar{v}(-\mathbf{k}, s), \quad (21)$$

and perform this decomposition on Eq. (8). In the shorthand notation $\chi_+^s \equiv u(\mathbf{k}, s)$ and $\chi_-^s \equiv v(-\mathbf{k}, s)$, the trace of Eq. (12) now reads (Dirac indices explicitly shown and implicitly summed over)

$$\begin{aligned} & \sim \sum_{s,r} \sum_{a,b=\pm} f_a f_b [\mathcal{P} + \beta]_{ij} [\chi_a^s]_j [\bar{\chi}_a^s]_k [\bar{\Gamma}^{\mu}]_{kl} [\not{p} + m]_{lm} \\ & \quad \times [\Gamma^{\nu}]_{mn} [\chi_b^r]_n [\bar{\chi}_b^r]_i. \end{aligned} \quad (22)$$

By inspection, this can be cast in the form

$$H_{\text{RPWIA}}^{\mu\nu} = (2\pi)^3 M_d \sum_{\text{spins}} \sum_{a,b=\pm} \rho_{ab;rs} \mathcal{H}_{ab;rs}^{\mu\nu}. \quad (23)$$

A *weak* form of factorization, therefore, still holds, with momentum distribution $\rho_{ab;rs}$ now being a density matrix in both spin and energy projection indices

$$\rho_{ab;rs} = f_a f_b \frac{m^2}{6\pi^3 M_d (k^2 - m^2)^2} \text{Tr} \left\{ \chi_a^s \bar{\chi}_b^r \frac{\not{p} + \beta}{2m} \right\}, \quad (24)$$

and similarly for the single-nucleon tensor

$$\mathcal{H}_{ab;rs}^{\mu\nu} = \text{Tr} \left\{ \chi_b^r \bar{\chi}_a^s \bar{\Gamma}^{\mu} \frac{\not{p} + m}{2m} \Gamma^{\nu} \right\}. \quad (25)$$

Using $v(-\mathbf{k}, s) = \gamma^5 \gamma^0 u(\mathbf{k}, s)$ and [30]

$$u(\mathbf{k}, s) \bar{u}(\mathbf{k}, r) = \frac{\bar{\mathbf{k}} + m}{2m} \frac{\delta_{s,r} + \gamma^5 \not{\xi}_{s,r}}{2}, \quad (26)$$

where $\xi_{s,r}^{\mu} = \bar{u}(\mathbf{k}, r) \gamma^5 \gamma^{\mu} u(\mathbf{k}, s)$, we find

$$\rho_{\pm\pm;rs} = \delta_{s,r} f_{\pm}^2 \frac{(k_{\pm} \cdot \mathcal{P}) \pm m\beta}{12\pi^3 M_d (k^2 - m^2)^2} \quad (27)$$

$$\begin{aligned} \rho_{+-;rs} &= f_+ f_- \frac{\bar{E}_k (\xi_{s,r} \cdot \mathcal{P}) - [(k_+ \cdot \mathcal{P}) + m\beta] \xi_{s,r}^0}{12\pi^3 M_d (k^2 - m^2)^2} \\ &= \rho_{-+;rs}. \end{aligned} \quad (28)$$

Thus, the diagonal terms $(+, +)$ and $(-, -)$ are diagonal in spin indices as well. Setting

$$\rho_{\pm\pm;rs} = \rho_{\pm\pm} \delta_{r,s}, \quad \sum_{\text{spins}} \delta_{r,s} \mathcal{H}_{\pm\pm;rs}^{\mu\nu} = \mathcal{H}_{\pm\pm}^{\mu\nu}, \quad (29)$$

we obtain for the diagonal contributions

$$\sum_{\text{spins}} \rho_{\pm\pm;rs} \mathcal{H}_{\pm\pm;rs}^{\mu\nu} = \rho_{\pm\pm} \mathcal{H}_{\pm\pm}^{\mu\nu}, \quad (30)$$

where we make use of $\sum_s \xi_{s,s}^{\mu} = 0$ to identify $\mathcal{H}_{++}^{\mu\nu} = \mathcal{H}_{\text{FPWIA}}^{\mu\nu}$ [cf. Eq. (15)], $\rho_{++} = f_+^2 [m\beta + (\bar{\mathbf{k}} \cdot \mathcal{P})] / 12\pi^3 M_d (k^2 - m^2)^2$, and analogously for the $(-, -)$ contribution. The observation made in Eq. (18) can thus be formally stated as follows: the first step (actually the *only* step, as shown below) required for the reduction to FPWIA [cf. Eq. (16)] is a projection to $(+, +)$ energy sector. With respect to the off-diagonal (in energy indices, $a \neq b$) contribution, notice that the relevant momentum distribution does not appear to be diagonal in spin space either. The second term in Eq. (17), which, as noted above, spoils strong factorization, is an off-diagonal energy $(+, -)$ term, as suggested by writing

$$m^2 - k^2 = \bar{E}_k^2 - E_k^2 = -2f_+ f_- [m^2 + (\bar{\mathbf{k}} \cdot \boldsymbol{\eta})]. \quad (31)$$

This is verified by explicit evaluation in Appendix B.

C. Nonrelativistic Momentum Distribution

We now address the relationship between ρ_{++} and the familiar, nonrelativistic deuteron momentum distribution $\rho(|\mathbf{k}|) \sim [u^2(|\mathbf{k}|) + w^2(|\mathbf{k}|)]$. In terms of the wavefunctions u , w , v_s and v_t , the vertex functions in Eq. (7) are given by [14]

$$\begin{aligned} A &= \mathcal{N} \left[u - \frac{1}{\sqrt{2}} w + \frac{m}{|\mathbf{k}|} \sqrt{\frac{3}{2}} v_t \right] \\ B &= \mathcal{N} \left[\frac{m}{\bar{E}_k + m} u + \frac{m(2\bar{E}_k + m)}{\sqrt{2}|\mathbf{k}|^2} w + \frac{m}{|\mathbf{k}|} \sqrt{\frac{3}{2}} v_t \right] \\ G &= \frac{2\mathcal{N}m^2}{M_d} \left[\frac{u}{\bar{E}_k + m} - \frac{\bar{E}_k + 2m}{\sqrt{2}|\mathbf{k}|^2} w \right] + 2\pi \sqrt{6M_d} \frac{m^2}{|\mathbf{k}|} v_s \\ F &= -2\pi \sqrt{2M_d \bar{E}_k} \sqrt{\frac{3}{2}} \frac{m}{|\mathbf{k}|} v_t, \end{aligned} \quad (32)$$

where $\mathcal{N} = \pi\sqrt{2M_d}(\bar{E}_k - E_k)$. Intuitively, we expect that ρ_{++} reduces to ρ in the nonrelativistic limit, that is, by ignoring the P states, and, additionally, making a $(|\mathbf{k}|/m)^2$ expansion [31]. It turns out, however, that neither approximation is necessary, and, in fact, ρ_{++} and ρ are *identical*. To see this, first notice that the overall contribution of the P states must cancel out once the projection to the $(+, +)$ sector is made, since such states represent “lower” Dirac components ψ^- of the deuteron wavefunction: from Eq. (38) in Ref. [14] we have (in our notation)

$$\begin{aligned} {}^3S_1, {}^3D_1 &\in \psi^+ \sim \bar{\chi}_+(\mathcal{X}\cdot\xi)v(n) \\ {}^3P_1, {}^1P_1 &\in \psi^- \sim \bar{\chi}_-(\mathcal{X}\cdot\xi)v(n) . \end{aligned} \quad (33)$$

By construction, the $(+, +)$ sector does not contain χ_- terms. Thus, ρ_{++} is oblivious to the P states (we have verified this numerically, as well), which can therefore be neglected for the purposes of writing ρ_{++} in terms of wavefunctions. Notice that, although in this case $F \rightarrow 0$, there is still an apparently nonvanishing contribution to ρ_{++} from the “off-shell” vertex function G ; however, this can be shown to vanish identically. For example, from Eqs. (A2) and (A3) in the appendices, and using Eq. (32), we have for the G^2 terms in the deuteron rest frame

$$\begin{aligned} \mathcal{O}(G^2) &\sim m^2 + k^2 + (k^2 - m^2)\frac{(\bar{k}\cdot n)}{m^2} - 2(k\cdot\bar{k}) \\ &\quad + 2(k\cdot n) - 2(k\cdot n)\frac{(k\cdot\bar{k})}{m^2} \\ &= m^2 + E_k^2 + 2E_k\bar{E}_k + (E_k^2 - \bar{E}_k^2)\frac{\bar{E}_k^2 + |\mathbf{k}|^2}{m^2} \\ &\quad - \frac{2}{m^2}(\bar{E}_k^2 E_k^2 - |\mathbf{k}|^4) - 2\bar{E}_k E_k + 3|\mathbf{k}|^2 \\ &= m^2 - 2\frac{\bar{E}_k^4}{m^2} + \bar{E}_k^2 + 3|\mathbf{k}|^2 + 2\frac{|\mathbf{k}|^4}{m^2} \\ &= 0 , \end{aligned} \quad (34)$$

and similarly for the AG and BG terms. Thus, once the P states have been shown to decouple, the nonvanishing contribution comes from the A and B vertex functions alone. From Eq. (A2) and Eq. (A3) with $\mathcal{D}^2 = -|\mathbf{k}|^2$, we find

$$\begin{aligned} m\beta + \bar{k}\cdot\mathcal{P} &= A^2(3m^2 + 3(n\cdot\bar{k}) - 2(N\cdot\bar{k})) \\ &\quad + B^2\frac{\mathcal{D}^2}{m^2}(m^2 - (n\cdot\bar{k})) - 2AB((\mathcal{D}\cdot n) - (\mathcal{D}\cdot\bar{k})) \\ &= A^2(6m^2 + 4|\mathbf{k}|^2) + 4AB|\mathbf{k}|^2 + 2B^2\frac{|\mathbf{k}|^4}{m^2} . \end{aligned} \quad (35)$$

To leading nonrelativistic order we find from Eq. (35) and Eq. (32) (without $v_t!$)

$$m\beta + \bar{k}\cdot\mathcal{P} = \mathcal{N}^2 \left[6m^2 \left(u - w/\sqrt{2} \right)^2 + 9m^2 w^2 \right.$$

$$\left. + 12m^2 \left(u - w/\sqrt{2} \right) w/\sqrt{2} \right] = 6\mathcal{N}^2 m^2 (u^2 + w^2) . \quad (36)$$

After some suppressed algebra we find that retaining all terms modifies Eq. (36) multiplicatively, by \bar{E}_k^2/m^2 . Thus, we finally obtain

$$\begin{aligned} m\beta + \bar{k}\cdot\mathcal{P} &= 6\mathcal{N}^2 \bar{E}_k^2 (u^2 + w^2) \\ \Rightarrow \rho_{++} &= f_+^2 \frac{m\beta + (\bar{k}\cdot\mathcal{P})}{12\pi^3 M_d (k^2 - m^2)^2} \\ &= \frac{6\mathcal{N}(\bar{E}_k + E_k)^2 \bar{E}_k^2 (u^2 + w^2)}{48\pi^3 M_d \bar{E}_k^2 (k^2 - m^2)^2} \\ &= \frac{u^2 + w^2}{4\pi} , \end{aligned} \quad (37)$$

where we have used Eq. (20) and $k^2 - m^2 = E_k^2 - \bar{E}_k^2$. ρ_{++} is precisely the nonrelativistic momentum distribution, apart from an overall normalization, since, when P states are present, ρ_{++} is not suitably normalized, i.e., $\int_0^\infty d\kappa \kappa^2 [u^2 + w^2] < 1$. Before proceeding to the next section, two comments seem appropriate. First, it is important that ρ_{++} contains $\bar{k}\cdot\mathcal{P}$, rather than $k\cdot\mathcal{P}$. This can be seen by observing that the leading order coefficient of the B^2 term must be $\sim |\mathbf{k}|^4$, otherwise ρ_{++} diverges as $|\mathbf{k}| \rightarrow 0$ [cf. Eq. (32)]. Using $k\cdot\mathcal{P}$ would add to the RHS of Eq. (35) a term $B^2 |\mathbf{k}|^2 \bar{E}_k (E_k - \bar{E}_k)/m^2$, which, because of the deuteron binding energy b , would diverge as $|\mathbf{k}| \rightarrow 0$, since $\bar{E}_k - E_k = |b| + \mathcal{O}(|\mathbf{k}|^2/m^2)$. Second, we emphasize that Eqs. (34) and (35) are only valid *after* the overall contribution of P states has cancelled out. In other words, the F and G vertex functions do contribute in ρ_{++} when the P states are present; their contribution, though, serves to cancel that of the P states from the A and B terms.

IV. VALIDITY OF THE REDUCTION

A. Kinematical considerations

In the previous section it was shown that the de Forest type of factorized PWIA is obtained from the RPWIA by projecting onto the the positive energy sector of the propagating struck nucleon. The legitimacy of this projection depends on $f_+ \simeq 1$, $f_- \ll 1$: the more off-shell is the struck nucleon, the less valid the projection. Energy/momentum conservation at the d - p - \bar{n} vertex in the deuteron rest frame implies that the struck nucleon is off-shell by

$$\begin{aligned} \bar{E}_k - E_k &= 2\sqrt{m^2 + \mathbf{k}^2} - M_d \\ &= |b| + \frac{\mathbf{k}^2}{m} + \dots , \end{aligned} \quad (38)$$

where the ellipses denote higher order relativistic terms. The binding effect is negligible for the deuteron ($|b| \approx 2.22$ MeV) and $|\mathbf{k}|$ is effectively restricted by the small deuteron Fermi momentum ($k_F \approx 60$ MeV/c), resulting in a rapid falloff of the momentum distribution $\rho(|\mathbf{k}|)$. The projection seems, therefore, meaningful (at least in the deuteron rest frame). Some caution must be exercised, however, for two reasons. First, there may be cases, where, despite $f_+ \simeq 1$, backward propagation is essential. An example is low energy Compton scattering from, e.g., a proton, where, to leading order, forward propagation cancels between the s and u channels and the classical (Thomson) limit is entirely due to the backward propagation terms [29]. Second, the applicability of the Fermi motion argument depends on the kinematics (choice of energy transfer ω for fixed momentum transfer $|\mathbf{q}|$), which determines the integration region for inclusive scattering [cf. Eq. (13)]. Overall energy/momentum conservation implies [18,30] for the integration limits $k_{\min} = |y|$, $k_{\max} = Y$

$$y(|\mathbf{q}|, \omega) = (M_d + \omega) \sqrt{\frac{1}{4} - \frac{m^2}{s} - \frac{|\mathbf{q}|}{2}}, \quad (39)$$

and $Y = y + |\mathbf{q}|$, with $s \equiv (M_d + \omega)^2 - |\mathbf{q}|^2$. On the quasielastic peak ($\omega = \omega_{qe}$)

$$\begin{aligned} M_d + \omega_{qe} &= \sqrt{m^2 + |\mathbf{q}|^2} + m \\ \Rightarrow \omega_{qe} &= \frac{q^2}{2m} + \mathcal{O}(|b|) \end{aligned} \quad (40)$$

the lower limit $|y| = 0$, and, therefore, the contribution of small momentum components $|\mathbf{k}|$ saturates the nuclear response in Eq. (13). Higher momentum components contribute as well, however, their importance (as weighted by the rapidly falling momentum distribution), is negligible. Away from the quasielastic peak, though, $y \neq 0$. As an extreme example consider the situation at threshold, where $s = 4m^2$, and thus

$$\begin{aligned} M_d + \omega_{thr} &= \sqrt{4m^2 + |\mathbf{q}|^2} \\ \Rightarrow \omega_{thr} &= \frac{q^2}{4m} + \mathcal{O}(|b|). \end{aligned} \quad (41)$$

In this case $|y| = |\mathbf{q}|/2$, and the struck nucleon will be off-shell by $1 - E_k/\bar{E}_k \geq (2 - M_d/\sqrt{m^2 + y^2})$, which, near threshold, translates into 24%, 63% and 115% for typical TJNAF processes with $|\mathbf{q}|=1$, $|\mathbf{q}|=2$ and $|\mathbf{q}|=4$ GeV/c, respectively.

B. Electromagnetic responses and the cross section

The effects of the projection on the longitudinal (R_L) and transverse (R_T) responses entering the inclusive cross section can be seen in Figs. 2–6. The

responses are decomposed into $(+, +)$, $(+, -)$ and $(-, -)$ contributions, after carrying out the spin summation in Eq. (23). By $(+, -)$ we denote the total off-diagonal contribution, i.e., $(+, -)$ plus $(-, +)$ in the notation of Eq. (23). Unlike the $(+, +)$ and $(-, -)$ contributions which are always positive in the case of the electromagnetic responses, the off-diagonal ones appear with either sign. For numerical evaluation, it is easier to project directly from Eq. (12) by applying the decomposition (19) to Eq. (10), and then use $f_+ - f_- = 1$ to arrange the resulting expression in f_+^2 , $f_+ f_-$ and f_-^2 terms. We have verified that this is identical to the direct trace evaluation of Eq. (23) described in Sect. III and Appendix B.

The residual relativistic effects we are interested in correspond to the difference between RPWIA and FPWIA results. From the discussion of the previous section follows that the R^{++} responses are identical with the FPWIA ones modulo an overall normalization, since $\int d\kappa \kappa^2 (u^2 + w^2) < 1$ when P states are present, while in FPWIA one uses wavefunctions normalized to unity. This results to a maximum 1.4% effect (with the $\lambda = 1$ vertex functions, see below). In the case of the PV asymmetry, where such 1% differences are important, this renormalization is irrelevant, as it cancels in the ratio of cross sections. Thus, in the following we use the terms $(+, +)$ -projected and FPWIA interchangeably.

We present results for $|\mathbf{q}| = 0.3$ GeV/c, representative of a low energy experiment such as the SAMPLE project, and $|\mathbf{q}| = 1$ GeV/c, representative of a medium energy experiment at TJNAF. Current conservation has been enforced (“cc”) by eliminating J^3 , as discussed in Sec. III. For the on-shell form factors appearing in the electromagnetic vertices $\Gamma_{1,2}^\mu$ [cf. Eq. (14)], we assume that they will be experimentally well known by the time the PV measurements will have been completed, and thus use the parametrization in Refs. [32,33] rather than model calculations. In this parametrization $G_E^p = (1 + 4.97\tau)^{-2}$, $G_M^{p,n} = \mu_{p,n} G_E^p$ and $G_E^n = -\tau G_M^n (1 + 5.6\tau)^{-1}$, with $\tau = |q^2|/4m^2$ and where $\mu_p = 2.79$, $\mu_n = -1.91$ are the proton and neutron anomalous magnetic moments, respectively. For the four vertex functions in the d-p- \bar{n} vertex we use the spectator equation solutions obtained by Buck and Gross [14]. These solutions are labelled by a parameter λ that interpolates between pseudovector ($\lambda = 0$) and pseudoscalar ($\lambda = 1$) πNN coupling

$$-ig_p \bar{\psi} \left[\lambda - i(1 - \lambda) \frac{\not{q}}{2m} \right] \gamma_5 \phi \psi. \quad (42)$$

From the interpretation of the P states as lower Dirac components of the deuteron wavefunction, one expects that pseudoscalar (ps) coupling would enhance the role of the P states, since γ_5 , being off-diagonal, mixes lower and upper components. As discussed in

Ref. [14] this is indeed the case, and the importance of P states increases rapidly between $\lambda = 0$ (pv) and $\lambda = 1$ (ps).

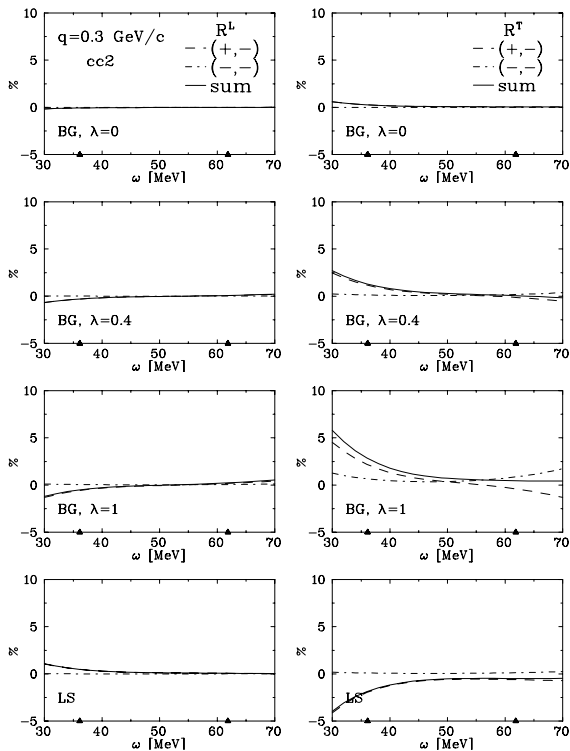


FIG. 2. Percentage decomposition of inclusive electromagnetic responses (left panels, R_L , right panels, R_T) using the Γ_2^μ vertex, at $|\mathbf{q}| = 300$ MeV/c. Dashes: $(+, -)$ contribution; dot-dashes: $(-, -)$ contribution; solid: total contribution of negative energy components, i.e., $1 - R^{++}/R$. Results shown for different choices of deuteron vertex functions. The solid triangles mark the quasifree region [cf. Eq. (44)].

Commensurate, looking at the “BG” panels in Figs. 2–5, we see that the difference between FPWIA and RPWIA, i.e., the error induced by projecting onto the $(+, +)$ sector, significantly increases with λ . It is well known, however, that the ps and pv πNN Lagrangians are related via a field redefinition (to lowest order in λ , at higher orders the field transformation generates contact terms, as well). According to basic field theory properties, the amplitude of the overall on-shell process should not depend on λ [34,23]. The fact that it actually does, partially reflects the inconsistency of computing the d-p- \bar{n} vertex functions in a specific model (both the on-shell, A , B and off-shell, F , G) ones, while not using the same model for the vertex functions of the photon-nucleon vertex. In particular, it is inconsistent to use the off-shell vertex functions F and G in the d-p- \bar{n} vertex of Eq. (7), while ignoring altogether the two extra vertex functions entering the half-off-shell γNN vertex.

As a side remark, one notices that, while realistic (in the sense that deuteron properties can be reproduced using them) model solutions have been obtained for F and G , first-principles calculations of the off-shell electromagnetic vertex functions are indicative rather than realistic [24]. Conceivably, this reflects the fact that in the deuteron off-shell vertex one needs the *constituent* off-shell, while, in the γNN off-shell vertex, one needs the *bound state* itself off-shell, which is, apparently, more difficult to describe.

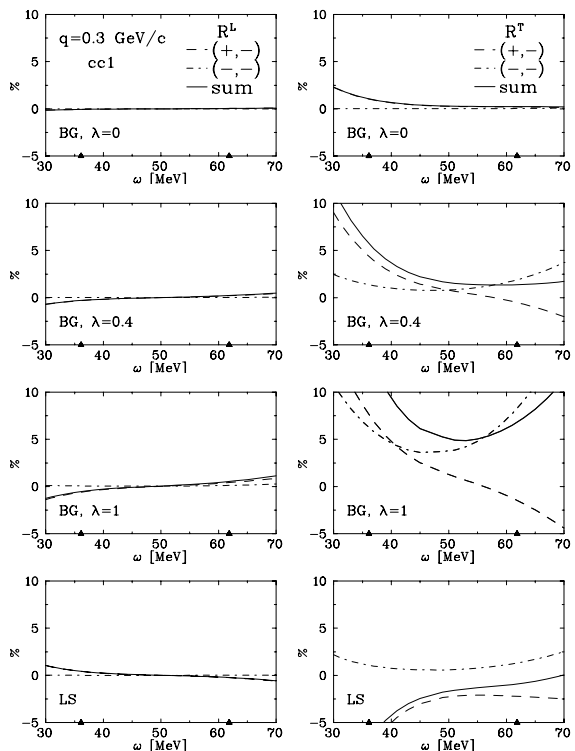


FIG. 3. As in Fig. 2, but with the Γ_1^μ vertex.

It appears, therefore, reasonable to ignore the off-shell vertex functions in the d-p- \bar{n} vertex, as long as only on-shell electromagnetic form factors are used. This point of view has been adopted, e.g., in Ref. [16], where a parametrization of the deuteron vertex by Locher and Svarc [35] using only the A and B vertex functions was employed. Since our primary motivation in this work is to investigate as widely as possible the extent to which effects associated with the relativistic aspects of the deuteron vertex modify the factorized PWIA, we will, nevertheless, use the off-shell deuteron vertex functions. In an attempt to partially alleviate the inconsistency of this scheme, we also show some results, whereupon we still use only two vertex functions for the γNN vertex, but modify the on-shell form factors according to

$$F(q^2, k^2) = F_{\text{Galster}}(q^2) \times \left[\frac{F_{\text{ps}}(q^2, k^2)}{F_{\text{ps}}(q^2, m^2)} \right], \quad (43)$$

allowing for a dependence on the other scalar variable, k^2 . For the modification factor we use the one-loop calculation with pseudoscalar (ps) πNN coupling of Naus and Koch [24]. Admittedly *ad hoc*, this procedure (first adopted in Ref. [36]) incorporates, nevertheless, what has been shown to be – within a toy model – the prominent feature of the EM half-off-shell vertex. For consistency, we only apply this modification scheme with the pseudoscalar ($\lambda = 1$) deuteron vertex functions. For comparison purposes, we also show some results in the Locher-Svarc scheme (labelled “LS”). We find, in general, that the effects of the projection are large in this scheme, comparable in magnitude to those with the $\lambda = 1$ Buck-Gross vertex functions.

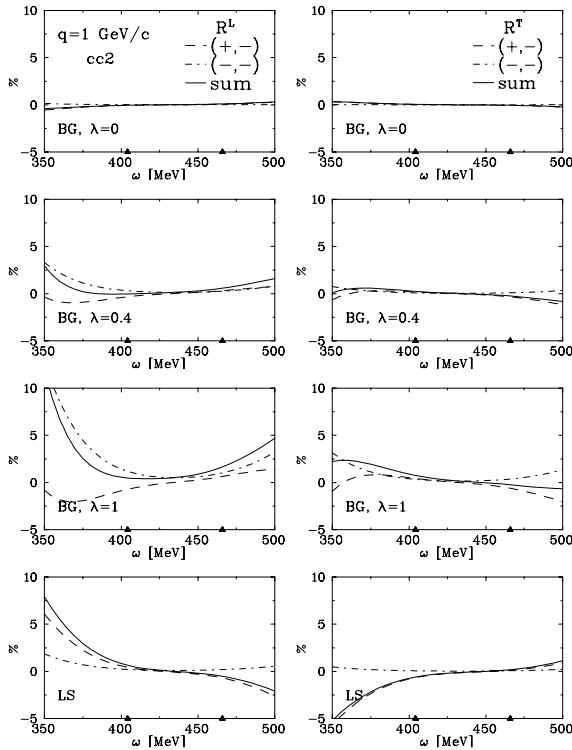


FIG. 4. As in Fig. 2, but at $|\mathbf{q}| = 1 \text{ GeV}/c$.

Looking at Figs. 2 and 3, one sees that at the low momentum transfer value ($|\mathbf{q}| = 300 \text{ MeV}/c$), the effects of neglecting negative ($-$) components in the longitudinal response, R_L , are negligible for all energy transfer values ω considered, independently of the deuteron vertices and form of the EM current operator used. For the transverse response, R_T , more significant effects are seen, particularly with the Γ_1^μ vertex. Specifically, with the Γ_2^μ vertex (Fig. 2) the effects increase with λ but are still below 2% inside the quasielastic ridge

$$|w - w_{qe}| < \sqrt{2}k_F|\mathbf{q}|/2\sqrt{m^2 + |\mathbf{q}|^2}. \quad (44)$$

For the Γ_1^μ vertex, however, 5-10% effects are seen (Fig. 3), especially with the $\lambda = 1$ vertex functions. In all cases, the effects are minimal for quasifree kinematics, as anticipated from the discussion in the previous section. At this momentum transfer value, we find that a modification according to Eq. (43) does not produce an observable effect in the the $\lambda = 1$ panels of Fig. 3.

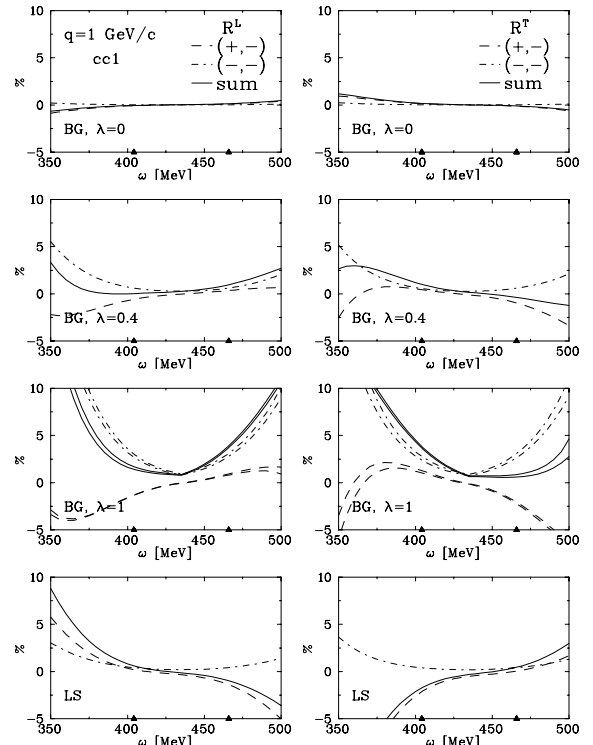


FIG. 5. As in Fig. 4, but with the Γ_1^μ vertex. In the $\lambda = 1$ panels results are shown with and without the modification of the on-shell form factors according to Eq. (43).

Unlike the case at the low momentum transfer, at $q = 1 \text{ GeV}/c$ (Figs. 4 and 5), R_L is affected by the projection more than R_T . Inside the quasifree region, though, the effects do not exceed 3% for either R_L or R_T . Thus, although the behavior of R_T is qualitatively similar to what happens at $|\mathbf{q}| = 300 \text{ MeV}/c$, the effects – particularly with cc1 – are, within the respective quasifree regions, *smaller* than at $|\mathbf{q}| = 300 \text{ MeV}/c$. This behavior does not contradict the remarks following Eq. (41), because threshold is close to the quasifree region at $|\mathbf{q}| = 300 \text{ MeV}/c$ (where $w_{thr} = 24 \text{ MeV}$), but not at $|\mathbf{q}| = 1000 \text{ MeV}/c$, where $w_{thr} = 250 \text{ MeV}$; that large effects are expected towards threshold can be seen by extrapolating the $\lambda = 1$ cc1 R_T panel in Fig. 5. This behavior in the quasifree region verifies that the *residual* relativistic

effects we describe are rather independent of the momentum transfer q^2 . If anything, they appear more important for low q^2 values, as can be also seen in Fig. 6, where the ratio of the $(+, +)$ -projected (i.e., FPWIA) to the full $(+, +) \oplus (+, -) \oplus (-, -)$ (i.e., RPWIA) responses is shown, for quasifree kinematics. The $\lambda = 1$ vertex functions are used, in order to display the maximum effect. The R_T response obtained with the Γ_1^μ EM vertex shows $> 2\%$ effects below $|\mathbf{q}| = 600$ MeV/c. At the SAMPLE kinematics ($|\mathbf{q}| = 300$ MeV/c) the effect on R_T^{cc1} is 5%.

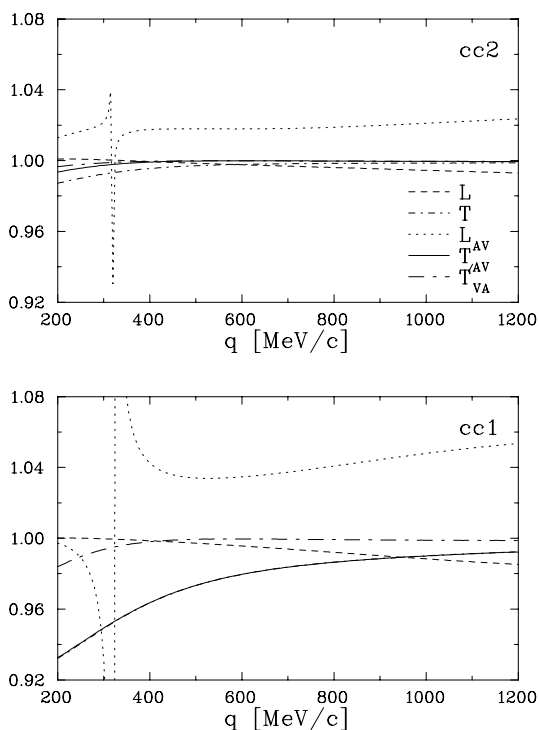


FIG. 6. The ratio R^{++}/R of electromagnetic (L, T) and parity-violating (L_{AV}, T_{AV}, T'_{VA}) responses accessible in inclusive $d(\vec{e}, e')$ scattering, for quasifree kinematics ($\omega = \omega_{qe}$) as a function of momentum transfer $|\mathbf{q}|$. The $\lambda = 1$ Buck-Gross deuteron vertex functions are used. Results are displayed for both cc1 and cc2 prescriptions for the single-nucleon tensor (the T and T_{AV} curves cannot be disentangled in the cc1 panel).

Returning to Fig. 5, note that the $(-, +)$ terms are not always dominant over the $(-, -)$ ones (see, e.g., the $\lambda = 1$ panels), as would have been expected given the extra suppression of the latter by f_-/f_+ . Finally, the $\lambda = 1$ results in Fig. 5 show an observable, but not dramatic change when the EM form factors are modified according to Eq. (43).

Turning to a direct comparison between cc1 and cc2 results, we write, using Eq. (14),

$$\bar{u}(p) [\Gamma_2^\mu - \Gamma_1^\mu] = \frac{F_2}{2m} \bar{u}(p) [(\Delta^\mu - \gamma^\mu \not{\Delta}) + \gamma^\mu (\not{\mathbf{k}} - m)], \quad (45)$$

where we have set $\Delta = \bar{k} - k = (\bar{E}_k - E_k, \mathbf{0})$. The Δ terms do not induce a large effect. In fact, they do not contribute anything when $\mu = 0$. In the FPWIA, the $(\not{\mathbf{k}} - m)$ term does not contribute because of the $(\not{\mathbf{k}} + m)$ projector onto the $(+, +)$ sector. Thus, the cc1 and cc2 longitudinal responses (both R^L and its parity-violating counterpart, R_{AV}^L) are *identical* in FPWIA [30,26] while the transverse ones differ, though not by much. This is not discernable from Figs. 2–6, but can be seen from Fig. 7, especially the inner plot, where the FPWIA cross sections differ insignificantly between cc1 and cc2 throughout the excitation energy region (solid line). The $(\not{\mathbf{k}} - m)$ term, however, contributes to the $(+, -)$ and $(-, -)$ parts of the RPWIA. It is therefore not surprising that a significant difference is seen in Fig. 7 between the cc1 and cc2 cross sections in RPWIA (dot-dashed line in inner plot) for non-quasifree kinematics, to be contrasted with the corresponding behavior after $(+, +)$ projection (FPWIA, solid line).

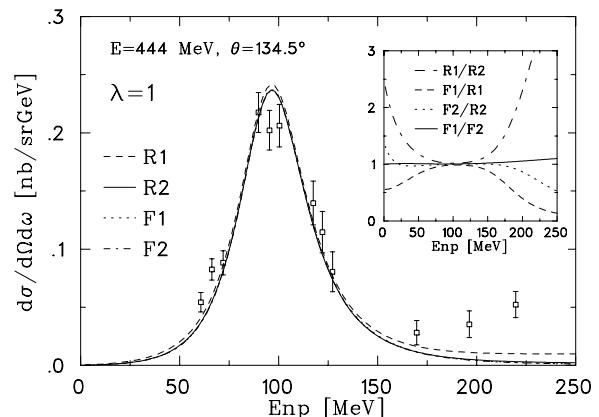


FIG. 7. Inclusive $d(e, e')$ cross section using the covariant (R_i) and $(+, +)$ -projected (F_i) responses, as a function of the final state excitation energy $E_{np} = \sqrt{(M_d + w)^2 - |\mathbf{q}|^2} - 2m$. The $\lambda = 1$ vertex functions and both $i = 1, 2$ EM vertex prescriptions are used. Ratios between different calculations are displayed in the inner graph. Data from Ref. [37].

Notice also, from the $\sigma_{cc1}^{++}/\sigma_{cc1}$ (labelled F_1/R_1) and $\sigma_{cc2}^{++}/\sigma_{cc2}$ (labelled F_2/R_2) ratios in the inner graph of Fig. 7, that the negative energy components play a larger role when the Γ_1^μ vertex is used. In fact, this is a common and rather unexpected feature of all Figs. 2–7: *the effect of the projection is more significant when cc1 is employed*. Given that either EM vertex amounts to an equally *ad hoc* choice, this observation cannot justify the overwhelmingly dominant use of the ‘cc1’ prescription in data analyses, if not

suggesting that relativistic effects are more appropriately incorporated when using cc2.

C. Parity-violating responses and asymmetry

In inclusive (\vec{e}, e') scattering of longitudinally polarized electrons (helicity $h = \pm 1$) from an unpolarized target, the asymmetry $A = (d\sigma^+ - d\sigma^-)/(d\sigma^+ + d\sigma^-)$ is purely parity-violating. There are two sources of parity-violation, electroweak ($\gamma - Z^0$) interference, and nuclear parity-violation. In the latter case, the weak interaction leads to a parity-violating component in the NN Hamiltonian, which allows parity mixture with P states (not to be confused with the relativistic P states discussed so far, which correspond to lower components of the coupled Dirac wavefunctions and therefore have the same *overall* parity as the S and D upper components [14]; these P states, on the other hand, arise in a nonrelativistic framework and have genuinely opposite parity). Nuclear parity-violation appears suppressed relatively to $\gamma - Z^0$ interference by α/α_s , where α_s denotes the strength of the (parity-conserving) strong interaction. In a recent calculation [38] the nuclear PV asymmetry appears, indeed, negligible (suppressed by three orders of magnitude) compared to the asymmetry due to electroweak interference over the whole range of momentum transfer values considered ($\mathbf{q} \in [0, 1000]$ MeV/c). Thus, in the following we focus on the PV asymmetry generated from the interference of electromagnetic (photon-exchange, A_γ) and neutral current (Z^0 -exchange, A_Z) amplitudes. In the one-boson approximation, and for momentum transfer values much smaller than the electroweak scale, $|q^2| \ll M_W^2$, the asymmetry is given by [33]

$$A = \frac{G|q^2|}{2\pi\alpha\sqrt{2}} \frac{a_A [v_L R_{AV}^L + v_T R_{AV}^T] + a_V v_T R_{VA}^{T'}}{v_L R_L + v_T R_T}. \quad (46)$$

Here G is the Fermi constant and $a_V(a_A)$ are the vector(axial-vector) couplings in the $e - Z^0$ vertex ($a_V\gamma_\mu + a_A\gamma_5\gamma_\mu$). To understand the $V - A$ structure of Eq. (46), it is useful to observe that the helicity ($h = \pm 1$) dependent part of the leptonic tensor $\tilde{l}^{\mu\nu}$ corresponding to the $A_\gamma - A_Z$ interference, reads

$$\tilde{l}^{\mu\nu} \equiv \sum_{h'} \langle e', h' | a_V \gamma_\mu + a_A \gamma_5 \gamma_\mu | e, h \rangle^* \langle e', h' | \gamma_\nu | e, h \rangle \sim h(a_{AS_{\mu\nu}} + ia_V a_{\mu\nu}) + [h\text{-independent}], \quad (47)$$

where $s_{\mu\nu}(a_{\mu\nu})$ are the symmetric(antisymmetric) parts of the leptonic tensor in Eq. (2), corresponding to the purely EM photon-exchange amplitude squared, $|A_\gamma|^2$ [30]. Analogously, we decompose the

hadronic tensor corresponding to the $A_\gamma - A_Z$ interference,

$$\tilde{H}^{\mu\nu} \equiv \overline{\sum}_{\text{spins}} \langle f | \hat{J}_{NC}^\mu | i \rangle^* \langle f | \hat{J}_{EM}^\nu | i \rangle, \quad (48)$$

into $\tilde{H}^{\mu\nu} = S^{\mu\nu} + iA^{\mu\nu}$. For unpolarized targets, an antisymmetric part $A^{\mu\nu}$ may only arise from axial-vector coupling. From general considerations in inclusive electron scattering [19] with polarized beam and unpolarized target, the L and T responses are generated by contracting the symmetric parts of the leptonic and hadronic tensors. Thus, from Eq. (47) the L and T parity-violating responses in the numerator of Eq. (46) arise from interference of the leptonic axial-vector with hadronic vector pieces (hence the AV index). The T' response, on the other hand, arises from contracting the antisymmetric tensors; it does not, therefore, contribute in unpolarized scattering – hence, does not enter the helicity sum in the denominator of Eq. (46) – and has a leptonic/vector with hadronic/axial-vector (VA) interference character. Thus, the nucleon axial-vector form factor $\tilde{G}_A^{T=1}$ that plays an important role in motivating these studies, as described in Sect. I, appears in the $R_{VA}^{T'}$ response. Notice, though, that since in the Standard Model $a_V = -1 + 4\sin^2\theta_W \simeq -0.092$, while $a_A = -1$, the $R_{VA}^{T'}$ response is effectively suppressed with respect to the other responses in electron scattering (but not in neutrino scattering, where $a_V = 1$ [33]).

The PV responses are computed from an interference hadronic tensor $\tilde{H}^{\mu\nu}$, analogous to the purely EM one in Eq. (8),

$$\tilde{H}_{\text{RPWIA}}^{\mu\nu} = \frac{4m^2}{3(k^2 - m^2)^2} \text{Tr} \left\{ \frac{\not{S} + T}{2m} \bar{\Gamma}_{NC}^\mu \frac{\not{p} + m}{2m} \Gamma_{EM}^\nu \right\}, \quad (49)$$

and then integrated according to Eq. (4). In a system of axes where the momentum transfer defines the z-axis and the y-axis is taken perpendicular to the hadronic plane defined by \mathbf{q} and \mathbf{k} , one has $W_{AV}^T = \tilde{H}^{11} + \tilde{H}^{22}$, $W_{VA}^{T'} = -2\text{Im}\tilde{H}^{12}$, and, in the “cc” treatment of current conservation, $W_{AV}^L = \tilde{H}^{00}$. In RPWIA we use, in direct analogy with Eq. (14), the momentum-space vertex operators

$$\Gamma_{NC,2}^\mu = \tilde{F}_1 \gamma^\mu + i \frac{q_\tau}{2m} \tilde{F}_2 \sigma^{\mu\tau} + \tilde{G}_A \gamma_5 \gamma^\mu$$

$$\Gamma_{NC,1}^\mu = (\tilde{F}_1 + \tilde{F}_2) \gamma^\mu - \frac{(k+p)^\mu}{2m} \tilde{F}_2 + \tilde{G}_A \gamma^\mu \gamma_5, \quad (50)$$

where we have not included terms corresponding to second-class currents [33]. An induced pseudoscalar axial-vector term $\tilde{G}_P q^\mu \gamma_5$ is possible and will generate a $\tilde{G}_P q^\mu [\dots]^\nu$ term in the hadronic tensor. Since axial contributions appear only in $W_{VA}^{T'} = -2\text{Im}\tilde{H}^{12}$,

though, and q^μ has vanishing 1 and 2 components, this term does not contribute.

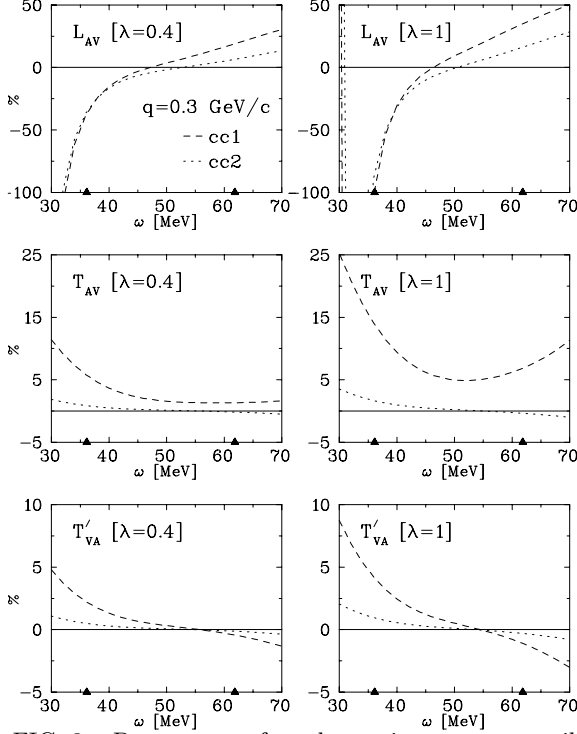


FIG. 8. Percentages of total negative-energy contribution ($1 - R^{++}/R$) to the parity-violating (L_{AV}, T_{AV}, T'_{VA}) responses computed in FPWIA (R^{++}) and RPWIA (R) with both cc1 (dashes) and cc2 (dots) at $|\mathbf{q}| = 300$ MeV/c. The $\lambda = 0.4(1)$ vertex functions are used in the left(right) panels. Notice the difference in scales.

In the Standard Model, the electromagnetic (EM) and weak neutral (NC) current operators (and therefore the corresponding nucleon form factors), are written as different linear combinations of elementary vector, $\bar{q}\gamma^\mu q$, and axial-vector, $\bar{q}\gamma^\mu\gamma_5 q$ (NC only), currents. Thus, considering three flavors ($q = u, d, s$) only, and using isospin symmetry, the NC form factors (in Sachs, $\tilde{G}_E = \tilde{F}_1 - \tau\tilde{F}_2$, $\tilde{G}_M = \tilde{F}_1 + \tilde{F}_2$, $\tau = |q^2|/4m^2$, representation) can be cast in the form [33,6]

$$\begin{aligned}\tilde{G}_{E,M}^{p,n} &= \left[\beta_V^p G_{E,M}^{p,n} + \beta_V^n G_{E,M}^{n,p} \right] - \frac{1}{2} G_{E,M}^s \\ \tilde{G}_A^{p,n} &= \beta_A^p G_A^{p,n} + \beta_A^n G_A^{n,p} - \frac{1}{2} G_A^s,\end{aligned}\quad (51)$$

where, at tree-level in the Standard Model,

$$\begin{aligned}\beta_V^p &= \frac{1}{2} (1 - 4 \sin^2 \theta_W) \\ \beta_V^n &= \beta_A^n = -\beta_A^p = -\frac{1}{2}.\end{aligned}\quad (52)$$

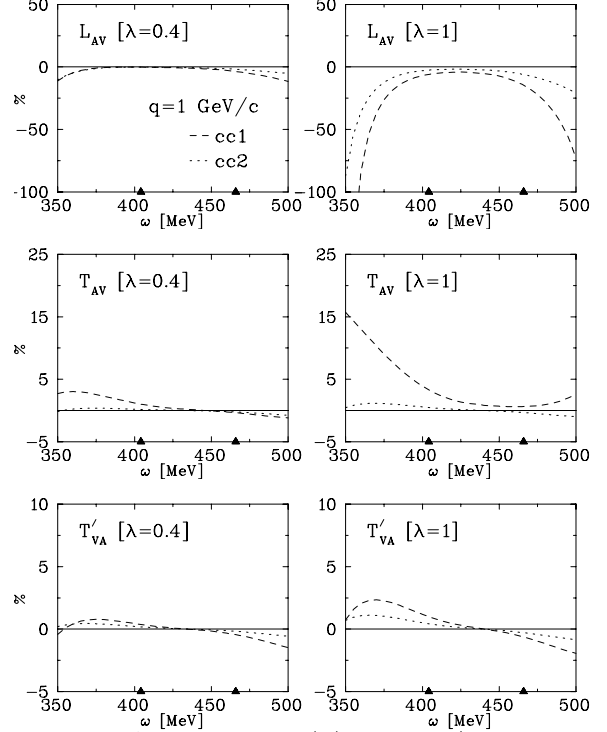


FIG. 9. As in Fig. 8, at $|\mathbf{q}| = 1$ GeV/c. Notice the difference in scales.

Provided the coefficients β are known (i.e., the radiative corrections small or reliably estimated) Eq. (51) implies that independent measurements of the EM and NC vector current nucleon matrix elements allows the experimental extraction of the hitherto unconstrained strangeness nucleon form factors $G_{E,M}^s$. The axial-vector form factors $G_A^{T=1} = G_A^p - G_A^n$, $G_A^{T=0} = G_A^p + G_A^n$ and G_A^s will also enter the parity-violating asymmetry A , through the $R_{VA}^{T'}$ response. Of those, $G_A^{T=0}$ does not contribute at tree-level, since, from Eq. (52), $\beta_A^{(0)} \equiv \beta_A^p + \beta_A^n = 0$. Any dependence on the (presumed small) G_A^s is practically eliminated due to the aforementioned suppression of $R_{VA}^{T'}$ by $a_V/a_A \simeq 10\%$ and has to be investigated using neutrinos [33]. Thus, only $G_A^{T=1}$ enters, but, as already mentioned, the large theoretical uncertainty in the radiative corrections to the associated coefficient $\beta_A^{(1)}$ makes its contribution crucial. Following Refs. [6,33], quantitative predictions are obtained by generalizing the Galster parametrization to include the extra form factors appearing in Eq. (51)

$$\begin{aligned}G_A^{T=1} &= g_A^{(1)} (1 + \lambda_A \tau)^{-2} \\ G_M^s &= \mu_s (1 + \lambda_s \tau)^{-2} \\ G_E^s &= \rho_s \tau (1 + \lambda_s \tau)^{-2},\end{aligned}\quad (53)$$

where, from β decay, at $\tau = 0$, $g_A^{(1)} = 1.26$, and we use $\lambda_A = 3.53$, $\lambda_s = 4.97$, i.e., equal to the Galster dipole

strength. Results in this section are with vanishing strangeness magnetic moment, μ_s , and strangeness radius, ρ_s [33].

In Figs. 8 and 9 we show the effects of the projection on the PV responses. For brevity, we show results only for two choices, $\lambda = 0.4$ (pv) and $\lambda = 1$ (ps), and, moreover, we do not show individual (+, -) and (-, -) decompositions, rather only the cumulative effect of the negative energy components. The behavior is similar to that of the parity-conserving, electromagnetic responses. Specifically, the effects of the projection are negligible with pseudovector coupling ($\lambda = 0$, not shown) for all responses and current prescriptions, and become more important as $\lambda \rightarrow 1$; in all cases the effects are minimal for quasifree kinematics; here, as well, the projection affects cc1 more severely than cc2; inside the quasielastic ridge, the effects are more pronounced at low momentum transfer, and as with the transverse response at $|\mathbf{q}| = 300$ MeV/c in Fig. 3, a potentially worrisome 5% effect is seen for the quasielastic R_{AV}^T cc1 response calculated with pseudoscalar coupling. The only essentially new feature comes from the parity-violating longitudinal response, R_{AV}^L , which appears extremely sensitive to the projection, especially towards threshold, with both $\lambda = 0.4$ and $\lambda = 1$ vertex functions at $|\mathbf{q}| = 300$ MeV/c, and, to a lesser extent, i.e., only with the $\lambda = 1$ ones, at $|\mathbf{q}| = 1$ GeV/c. This sensitivity, however, is not a consequence of large dynamical effects associated with negative energy components *per se*. Rather, it is an example of *any* subdominant effect playing an important role whenever the leading contribution vanishes (or becomes too small), as happens in this case because $\sin^2 \theta_W \simeq 1/4$. To see that, notice from Eq. (51) and the numerical values of the coefficients in Eq. (52) ($\beta_V^0 \approx 0.046$) that, although G_E^n is small compared to G_E^p (at least for $\tau < 1$), in the case of the neutral current (NC) it is the *neutron* form factor, \tilde{G}_E^n , that is much larger than the proton one, \tilde{G}_E^p . Consider then, from Eq. (A5) and Eq. (A6), the cc1 longitudinal response in FPWIA

$$\mathcal{W}_{VA}^{L,cc1} = \left[\frac{E_n + E_p}{2m} \right]^2 \sum_{p,n} \frac{\tilde{G}_E G_E + \tau \tilde{G}_M G_M}{1 + \tau} - \frac{|\mathbf{q}|^2}{4m^2} \sum_{p,n} \tilde{G}_M G_M + \mathcal{O}(\vec{k}^2 - k^2). \quad (54)$$

Using Eq. (51) and Eq. (52), and employing the Galster parametrization, we have

$$\frac{\mathcal{W}_{VA}^{L,cc1}}{[1 + \tau]^{-1} (G_E^p)^2} = \left[1 + \frac{\omega}{2m} \right]^2 \left(\beta_V^p + \frac{\mu_n \tau}{1 + 5.6\tau} \right) - \tau^2 \left(\beta_V^p [\mu_p^2 + \mu_n^2] - \mu_p \mu_n \right) \left[1 - \frac{\omega}{2m\tau} \right]^2. \quad (55)$$

where we have left out small contributions from off-

shell, strangeness, and $\tau \beta_V^p$ terms. The first term in Eq. (55) arises from the electric terms in Eq. (54), and the second from the magnetic terms. Because β_V^p is small, and the magnetic terms compete in Eq. (54), there is no dominant (i.e., $\mathcal{O}(1)$) term in the r.h.s. of Eq. (55). Thus, the parity violating longitudinal response is *small* in magnitude and appears with either positive or negative sign, depending on the kinematics.

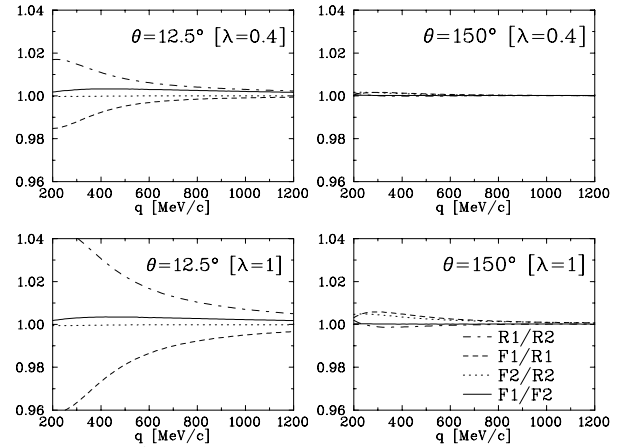


FIG. 10. Asymmetry ratios for quasifree kinematics, $\omega = \omega_{qe}$. Results presented for two choices of electron scattering angles θ and vertex functions λ . Notation as in Fig. 7.

Consider first quasifree kinematics, $\omega = q^2/2m$. In this case the second term in Eq. (55) vanishes (there are no magnetic contributions in the “static” approximation [6]). From the first term, it is clear that at low τ values (and thus low $|\mathbf{q}|$, since, for quasifree kinematics, $|\mathbf{q}| = 2m\sqrt{\tau(1 + \tau)}$) the quasielastic PV longitudinal response is positive and at higher τ negative, the sign reversing at $\tau = \beta_V^p / (1.91 - 5.6\beta_V^p) = 0.0278$, or $|\mathbf{q}| \simeq 317$ MeV/c. The exact kinematics where the sign flips will depend, of course, on the small effects not included in Eq. (55), as well as the projection effects [cf. Table. I]. Thus, around $|\mathbf{q}| = 320$ MeV/c the zeros in R_{AV}^L give rise to a discontinuous behavior of the the ratio of R_{AV}^L in FPWIA and RPWIA for quasifree kinematics, as indeed observed in Fig. 6. Interestingly enough, this momentum transfer value is very close to that of SAMPLE. SAMPLE, however, focusing on the magnetic strangeness form factor, is a backward angle measurement. At $\theta > 50^\circ$ the asymmetry is dominated by the T part, and, to a lesser extent – because of a_V being small – by the T' part. Thus, the PV longitudinal response, and the projection effects associated with it, do not affect the SAMPLE measurement.

Because of the behavior of R_{AV}^L , one expects that projection effects will depend strongly on the electron

scattering angle. For quasifree kinematics, this is evident from Fig. 10. At $|\mathbf{q}| = 300$ MeV/c, up to 4% effects in the forward asymmetry can be seen (this would be prohibitively large for strangeness studies), while at backward angles the asymmetry is very stable, showing a maximum in the $|\mathbf{q}| = 300$ MeV/c region, which is, nevertheless, less than 1%. Recall that, in this case, the individual R^T and R_{AV}^T transverse responses appearing, respectively, in the numerator and denominator of the asymmetry, show a $\mathcal{O}(5\%)$ projection effect with cc1 and $\lambda = 1$ [cf. Figs. 3, 8 and 6], even on the quasielastic peak. Due to the dominantly transverse character of the asymmetry at $\theta = 150^\circ$, however, these effects by-and-large cancel in the ratio, and at this angle the asymmetry shows the aforementioned $< 1\%$ variation. The extent to which such an effect may interfere with strangeness studies is examined in the next section. Fortunately, the projection effects become less than 1% for high enough momentum transfer even at forward angles, as, e.g., for a possible TJNAF Hall A measurement ($|\mathbf{q}| = 1$ GeV/c, $\theta = 12.5^\circ$) proposed in Ref. [6].

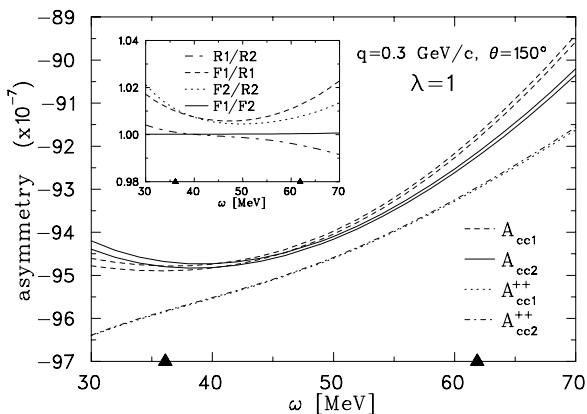


FIG. 11. The PV asymmetry at $|\mathbf{q}| = 300$ MeV/c and backward ($\theta = 150^\circ$) angle, using the $\lambda = 1$ Buck-Gross vertex functions. RPWIA results are shown with (lower) and without (upper curves) the modification of the on-shell form factors according to Eq. (43). Notation in inner graph as in Fig. 7.

Away from the quasielastic peak, the second term in Eq. (55) gives a negative definite contribution, with a coefficient that rises with q^2 . Thus, R_{AV}^L is still positive for low $|\mathbf{q}|$ (as e.g., at 300 MeV/c) and negative at large $|\mathbf{q}|$ (as e.g., at 1 GeV/c). It is always small, though, and, especially outside the quasielastic ridge, negative components constitute a significant part of the response, resulting in the behavior observed in Figs. 8 and 9. At such non-quasifree kinematics, however, R_{AV}^L is quite sensitive to other aspects of nuclear dynamics beyond PWIA, as well, as has been shown in studies of both deuterium (e.g., proton-neutron interference contributions [17]) and heavier nuclei [39].

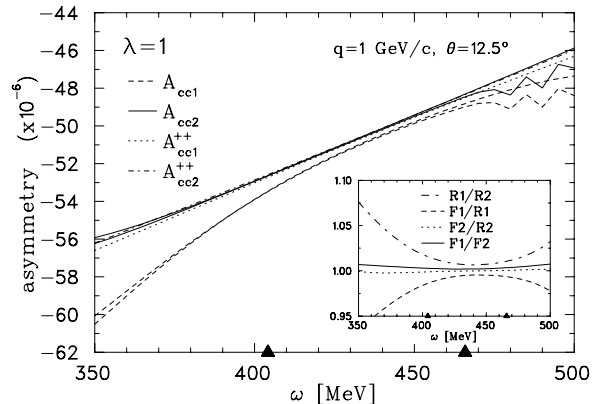


FIG. 12. As in Fig. 11, at $|\mathbf{q}| = 1$ GeV/c and forward ($\theta = 12.5^\circ$) angle.

In Figs. 11 and 12 we show the asymmetry in FPWIA and RPWIA, as well as the corresponding ratios, for the SAMPLE kinematics ($|\mathbf{q}| = 300$ MeV/c, backward angle) and a possible $|\mathbf{q}| = 1$ GeV/c forward angle measurement at TJNAF. The $\lambda = 1$ vertex functions are used to display the maximum effect of the projection. The residual relativistic effects associated with the relativistic treatment of the deuteron and the struck nucleon induce a less than 2% variation of the PV asymmetry within the quasielastic ridge. We also observe that the modification of the on-shell form factors to allow for a k^2 -dependence according to Eq. (43) amounts to a secondary effect (i.e., much smaller than the effect caused by the projection). An exception is observed at high ω values in the $|\mathbf{q}| = 1$ GeV/c case. This behavior is caused when deeply off-shell, $k^2 = \mathcal{O}(-m^2)$, momenta, for which Eq. (43) generates unreasonably large modification factors, contribute to the inclusive integral in Eq. (4). Since $k^2 = (M_d - \bar{E}_k)^2 - |\mathbf{k}|^2 \simeq 5m^2 - 4m\sqrt{m^2 + |\mathbf{k}|^2}$, values $k^2 = -m^2$ occur in the inclusive integral for $|\mathbf{k}| \geq 1.1m$. Such values are accessible for $|\mathbf{q}| > m$ and with increasing ω values, since above the quasielastic peak ($y > 0$) the upper integration limit $Y = y + |\mathbf{q}| > |\mathbf{q}|$.

Another qualitative difference between the two cases, is that while at $|\mathbf{q}| = 300$ MeV/c the behavior of cc1 is quite similar to that of cc2 on the quasielastic peak for both FPWIA (solid lines in inner graph of Fig. 11) and RPWIA (dot-dashes), at $|\mathbf{q}| = 1$ GeV/c we see (as we observed for the cross section before) that projection effects are larger for cc1 than cc2. At $|\mathbf{q}| = 300$ MeV/c the magnitude of the asymmetry is raised in going from RPWIA to FPWIA by about 0.5 – 1.5% with either cc1 or cc2 (Fig. 11), while at $|\mathbf{q}| = 1$ GeV/c (Fig. 12) there is an observable effect only for cc1, the magnitude of the asymmetry being reduced by 0.5 – 1% inside the quasielastic ridge.

D. Strangeness studies

Here we discuss the extent to which the residual relativistic effects associated with the projection affect the extraction of strangeness form factors from the PV $e-d$ asymmetry. We are primarily interested in the interplay between the magnetic strangeness form factor G_M^s and the NC axial isovector form factor $\tilde{G}_A^{T=1}$ (more precisely, the radiative corrections $R_A^{T=1}$ to the relevant coefficient $\beta_A^{(1)} = 1.26[1 + R_A^{T=1}]$). The approved SAMPLE and E91-017 experiments will attempt to extract both quantities by combining measurements of the $e-p$ and $e-d$ PV backward-angle asymmetries. In Fig. 13 we show “bands” of RPWIA and FPWIA results for SAMPLE kinematics, with $R_A^{T=1} = 0$ and for three values of the magnetic strangeness moment μ_s entering the *Ansatz* in Eq. (53), corresponding to zero strangeness ($\mu_s = 0$), the pole model result of Jaffe ($\mu_s = -0.3$) [40] and an unlikely high value ($\mu_s = -1$). Within each μ_s “band”, the projected (FPWIA) results show negligible variation (0.03% on the peak) between different calculations (i.e., cc1 *vs.* cc2 and $\lambda = 1$ *vs.* $\lambda = 0.4$). The variation induced when P states and negative energy components are included is small, but not negligible. Although the $\mu_s = 1$ and $\mu_s = 0$ bands are well separated, outside the quasielastic ridge the $\mu_s = 0$ and $\mu_s = -0.3$ bands overlap. As hoped, though, they have a minimum width for quasifree kinematics. This width depends, of course, on λ , as is evident from Fig. 13: the $\lambda = 0.4$ (long-dashes) cc1 RPWIA curves are much closer to the overlapping upper FPWIA curves compared to the $\lambda = 1$ (solid) ones. On the quasielastic peak, the maximum variation is observed between the projected and unprojected $\lambda = 1$ cc1 curves, amounting to a 0.56% effect. The asymmetry is linear in μ_s , $A(\mu_s) = A(0)[1 - b_\mu \mu_s]$, with $b_\mu = 0.057(1)$ in our models. Although b_μ is approximately tenfold the sensitivity to projection effects, it may not be large enough if μ_s turns out to be rather smaller than the pole value (something not excluded from other calculations [40]), to the extent, of course, that the widths observed in Fig. 13 give a measure of the theoretical nuclear physics uncertainty in describing the $e-d$ reaction.

In view of the rather small sensitivity of the $e-d$ asymmetry to G_E^s , the current consensus is to use the deuteron as a means of constraining the large theoretical uncertainty in $R_A^{T=1}$, using primarily the proton for extracting G_M^s . Accordingly, in Fig. 14 we fix the strangeness magnetic moment to the pole model value, and show “bands” of quasifree kinematics results, at tree level, $R_A^{T=1} = 0$, as well as two other values corresponding to the extrema in the calculation of Ref. [5], $R_A^{T=1} = -0.34 \pm 0.28$ [4]. It is evident that significant constraints can be placed on $R_A^{T=1}$ from a

measurement of the asymmetry and that the residual relativistic effects discussed here should not inhibit this procedure. Comparing the $|\mathbf{q}| = 300$ MeV/c and $|\mathbf{q}| = 1$ GeV/c regions, however, it appears that a higher q^2 measurement than that of SAMPLE (as for example in the E91-017 TJNAF experiment [3]) will place tighter constraints on $R_A^{T=1}$. Specifically, since the asymmetry is linear in \tilde{G}_A , we may write $A(\mu_s, R_A^{T=1}) = A(\mu_s, 0)[1 + b_A R_A^{T=1}]$. At $|\mathbf{q}| = 300$ MeV/c, the typical variation between models is $\Delta_{th} = 0.56\%$, while the sensitivity to the radiative corrections $b_A = 0.235(4)$. On the other hand, at $|\mathbf{q}| = 1050$ MeV/c we find a smaller $b_A = 0.1259(1)$, but also considerably reduced model variation, $\Delta_{th} = 0.1\%$. From the $A(\mu_s, 0)$ values we find that the difference between the $R_A^{T=1} = 0$ and $R_A^{T=1} = -0.06$ bands (upper two ones in Fig. 14) is $2.4\Delta_{th}$ at $|\mathbf{q}| = 300$ MeV/c, but roughly three times more effective, $7\Delta_{th}$, at $|\mathbf{q}| = 300$ MeV/c.

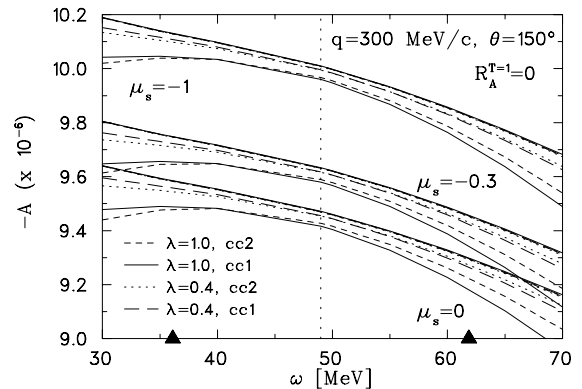


FIG. 13. The PV asymmetry at $|\mathbf{q}| = 300$ MeV/c and $\theta = 150^\circ$. Results shown for 3 values of the strangeness magnetic moment μ_s and 2 choices of Buck-Gross vertex functions λ . For each (μ_s, λ) choice, results are shown with both cc1 and cc2 for RPWIA (lower) and FPWIA (upper, practically indistinguishable curves). The quasielastic peak is marked by the dotted vertical line.

TABLE I. Momentum transfer $|\mathbf{q}_{cr}|$ in MeV/c where R_{AV}^T becomes negative (quasifree kinematics, $\mu_s = -0.3$). Results shown using: the static estimate in Eq. (56), factorized (F) cc1, and covariant (R) PWIA cc1 with the $\lambda = 1$ vertex functions.

ρ_s	1.5	0.5	0	-0.5	-1.0	-1.2	< -1.4
R_{cc1}	259	295	321	360	430	493	—
F_{cc1}	258	294	320	357	422	476	—
Eq. (56)	257	292	317	354	417	465	—

In the previous section we discussed the sign-reversing behavior of the PV longitudinal response R_{AV}^L in the absence of strangeness. For quasifree kinematics, where the magnetic terms cancel, only G_E^s enters, and a negative value of the strangeness radius modifies significantly this behavior. Using Eq. (53), Eq. (55) at $\omega = 2m\tau$ now becomes

$$\mathcal{W}_{VA}^{L,cc1} \sim \left(\beta_V^p + \frac{\mu_n\tau}{1+5.6\tau} - \tau \frac{\rho_s}{2} \left[1 - \frac{\mu_n\tau}{1+5.6\tau} \right] \right). \quad (56)$$

The resulting quadratic equation gives an estimate of the momentum transfer value $|\mathbf{q}_{cr}|$ where R_{AV}^L reverses sign as a function of ρ_s . As seen from Table I, this “static” estimate is reasonably accurate. For positive strangeness radius $|\mathbf{q}_{cr}|$ depends mildly on ρ_s , but for negative values $|\mathbf{q}_{cr}|$ becomes significantly larger and for $\rho_s < -1.4$ (the pole model value is -2.1 ± 1.0) the response is always positive.

Thus, given the large variation in the model predictions of ρ_s [40], a determination of R_{AV}^L in different $|\mathbf{q}|$ values might be helpful in constraining ρ_s . Although quite challenging, a separation of the L , T and T' parts of the PV asymmetry is not beyond current experimental capabilities, and will be performed for the $e-p$ PV asymmetry as part of the E91-017 TJNAF experiment [33].

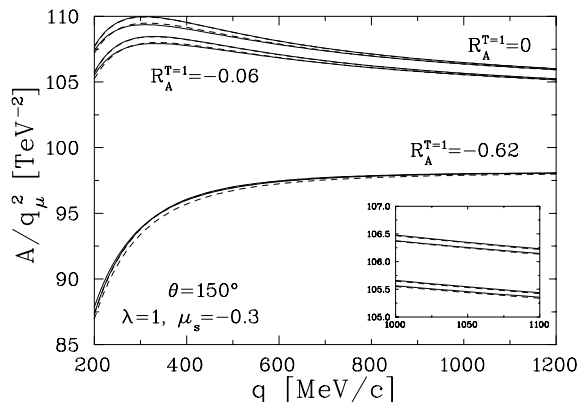


FIG. 14. The PV asymmetry [in units of q^2] as function of momentum transfer $|\mathbf{q}|$ for quasifree kinematics and $\theta = 150^\circ$. Results shown for 3 values of $\beta_A^{(1)}$ (see text). Solid lines: cc1, dashes: cc2. A magnification of the 1 GeV/c region is shown in the inner graph.

V. SUMMARY

In this work parity-violating, electron-deuteron scattering in the quasifree region has been studied in relativistic PWIA. The emphasis has been to quantify the role of residual relativistic effects associated with the non-relativistic treatment of the bound state in

the semirelativistic, factorized PWIA, assuming that the latter correctly incorporates relativistic effects associated with the large momentum transfer. The main results of this investigation can be summarized as follows:

- In the covariant calculation (RPWIA), factorization is spoiled by off-shell contributions associated with the struck nucleon. A weak factorization still holds, with the momentum distribution and the single-nucleon tensor being now density matrices in spin and energy-sign spaces of the struck nucleon. The familiar FPWIA using de Forest’s single-nucleon tensor corresponds to a projection of the RPWIA to the positive energy sector. That is, the $H_{++}^{\mu\nu}$ single-nucleon tensor is the FPWIA single-nucleon tensor, and the ρ_{++} momentum distribution is the nonrelativistic deuteron momentum distribution. No additional operations (such as neglect of P states that superficially appear in ρ_{++} , or nonrelativistic expansion) is required. Thus, this truncation defines the residual relativistic effects we are interested in, and shows the close connection between relativistic and off-shell effects. Similar considerations apply to quasielastic scattering on any nucleus and not just deuterium.
- Since, from the above, a covariant treatment of the $e-d$ scattering requires inclusion of off-shell effects, it is not consistent to incorporate such effects in the $d-n-p$ vertex but ignore them in the γNN and $Z^0 NN$ vertices. A measure of the thusly induced model dependence is obtained by using various on-shell-equivalent prescriptions for these vertices, and several model calculations for the deuteron vertex functions.
- The residual relativistic effects depend strongly on the πNN coupling used for calculating the deuteron vertex functions (minimal for pseudovector and maximal for pseudoscalar coupling). They also depend on the off-shell prescription for the nucleon vertex. Although the difference between cc1 and cc2 prescriptions is negligible in FPWIA, it is not such in RPWIA, where projection effects appear more pronounced with the cc1 prescription. In that respect, the cc2 prescription seems preferable.
- Effects associated with allowing for an off-shell dependence of the nucleon form factors are generically smaller than projection effects. The arbitrariness of the *Ansatz* used, however, does not allow definitive conclusions to be drawn.
- With the exception of the parity-violating longitudinal response, R_{AV}^L , inside the quasielastic

ridge the residual relativistic effects are below 5-10% with cc1, and a few % with cc2, when the pseudoscalar coupling (which maximizes such effects) is used. On the quasielastic peak, effects are typically below 2%. A notable exception is the $|\mathbf{q}| < 400$ MeV/c region where the transverse responses, R^T and R_{AV}^T , can have $> 4\%$ effects. The R_{AV}^L response can show quite important effects, especially in the $|\mathbf{q}| = 300$ MeV/c region, which reflect the lack of a dominant term in this response, thereby exposing otherwise non-leading contributions.

- The magnitude of these corrections for quasifree kinematics is small for them to play a role in the cross section. In the parity-violating asymmetry, where 1% effects are important for strangeness studies, the effects mostly cancel in the ratio. The R_{AV}^L response is sensitive to these effects and, thus, effects $> 2\%$ are seen in the forward angle asymmetry for $|\mathbf{q}| < 800$ MeV/c. For backward scattering, where the deuteron measurements will be used for disentangling the correlation between magnetic strangeness and axial-vector isoscalar radiative corrections, the PV asymmetry is sensitive to less than 1% to residual relativistic effects, the maximum sensitivity observed in the $|\mathbf{q}| = 300$ MeV/c region. Thus, the extraction of $\tilde{G}_A^{T=1}$ at the E91-017 TJNAF kinematics will be less sensitive to such effects than at the SAMPLE kinematics.

ACKNOWLEDGMENTS

I would like to thank Prof. J.A. Tjon for discussions that led to the formalism in Sect. III, Dr. A. Korchin for suggesting this calculation, and Dr. H.W.L. Naus for explaining certain features of the off-shell EM form factor. This work has been supported by Human Capital and Mobility Fellowship ERBCHBICT941430 and the Research Council of Australia.

-
- [1] Bates experiment # 89-06 (R. McKeown and D. Beck, contacts); Bates experiment # 94-11 (M. Pitt and E. Beise, contacts).
- [2] Mainz proposal # A4/1-93 (P. von Harrach, contact); F.E. Maas, to appear in Proceedings of the 12th International Symposium on High-Energy Spin Physics (SPIN96), Amsterdam, the Netherlands, 10-14 Sept. 1996.
- [3] TJNAF experiments: E91-017 (D. Beck, contact); E91-004 (E. Beise, contact); E91-010 (P. Souder, contact).
- [4] E.J. Beise et al., presented at 9th Amsterdam Miniconference on Electromagnetic Studies of the Deuteron, Amsterdam, Netherlands, 1-2 Feb 1996; archive: nucl-ex/9602001.
- [5] M. Musolf and B. Holstein, Phys. Lett. **242B**, 461 (1990).
- [6] E. Hadjimichael, G.I. Poulis and T.W. Donnelly, Phys. Rev C **45**, 2666 (1992).
- [7] The meson-exchange currents contribution is expected to be small for quasifree kinematics, see W. Fabian and H. Arenhövel, Nucl. Phys. **A314**, 253 (1979).
- [8] T. de Forest, Jr., Nucl. Phys. **A 392**, 232 (1983).
- [9] In recent work (J.E. Amaro, J.A. Caballero, T.W. Donnelly, A.M. Lallena, E. Moya de Guerra and J.M. Udias Nucl. Phys. **A602**, 263 (1996)) a new nonrelativistic expansion of the one body currents in $|\mathbf{k}|/m$ has been proposed in which relativistic kinematics are retained (i.e., no expansion in $|\mathbf{q}|/m$ is made). This expansion should greatly reduce the $> 6\%$ differences between the FSI and PWIA at TJNAF energies (in progress).
- [10] H. Göller and H. Arenhövel, Few Body Syst. **13**, 117 (1992).
- [11] B.D. Keister and J.A. Tjon, Phys. Rev. C **26**, 578 (1982).
- [12] E. Hummel and J.A. Tjon, Phys. Rev. C **49**, 21 (1994).
- [13] L.P. Kaptari, B. Kämpfer, A.Yu. Umnikov and F.C. Khanna, Phys. Lett. **351B**, 400 (1995).
- [14] W.W. Buck and F. Gross, Phys. Rev. D **20**, 2361, 1979.
- [15] R.G. Arnold, C.E. Carlson and F. Gross, Phys. Rev. C **21**, 1426 (1979).
- [16] G. Beck, T. Wilbois and H. Arenhövel, Few Body Syst. **17**, 91 (1994).
- [17] G.I. Poulis and T.W. Donnelly, Nucl. Phys. **A575**, 549 (1994).
- [18] D.B. Day, J.S. McCarthy, T.W. Donnelly and I. Sick, Ann. Rev. Nucl. Part. Sci. **40**, 357 (1990).
- [19] T.W. Donnelly and A.S. Raskin, Ann. Phys. **169**, 247 (1986).
- [20] R. Blankenbecler and L.F. Cook, Jr., Phys. Rev. **119**, 1745 (1960).
- [21] A. Bincer, Phys. Rev. **118**, 855 (1960).
- [22] S. Scherer and H.W. Fearing, Phys. Rev. C **51**, 359 (1995).
- [23] R.M. Davidson and G.I. Poulis, Phys. Rev. D **54**, 2228 (1996).
- [24] H.W.L. Naus and J.H. Koch, Phys. Rev. C **36**, 2459 (1987).
- [25] P.C. Tiemeijer and J.A. Tjon, Phys. Rev. C **42**, 599 (1990); X. Song, J.P. Chen and J.S. McCarthy, Z. Phys. **A 341**, 275 (1992).
- [26] J.A. Caballero, T.W. Donnelly and G.I. Poulis, Nucl. Phys. **A555**, 709 (1993).

- [27] S.J. Pollock, H.W.L. Naus and J. H. Koch, Phys. Rev. C **53**, 2304 (1996).
- [28] W. Melnitchouk, A.W. Schreiber and A.W. Thomas, Phys. Rev. D **49**, 1183 (1994).
- [29] S. Scherer, G.I. Poulis and H.W. Fearing, Nucl. Phys. **A570**, 686 (1994).
- [30] G.I. Poulis. Ph.D. thesis, Massachusetts Institute of Technology (1992).
- [31] G.I. Poulis, archive: hep-ph/9610536, to appear in Proceedings of the 12th International Symposium on High-Energy Spin Physics (SPIN96), Amsterdam, the Netherlands, 10-14 Sept. 1996.
- [32] S. Galster, H. Klein, J. Moritz, K.H. Schmidt, D. Wegener and J. Bleckwenn, Nucl. Phys. **B32** 221, 1971.
- [33] M.J. Musolf, T.W. Donnelly, J. Dubach, S.J. Pollock, S. Kowalski, E.J. Beise, Phys. Rep. **239**, 1 (1994).
- [34] S. Kamefuchi, L. O’Raifeartaigh and A. Salam, Nucl. Phys. **28**, 529 (1961).
- [35] M.P. Locher and A. Svarc, Z. Phys. **338**, 89 (1991).
- [36] H.W.L. Naus, S.J. Pollock, J.H. Koch and U. Oelfke, Nucl. Phys. **A509**, 717 (1990).
- [37] B.P. Quinn et al., Phys. Rev C **37**, 1609 (1988), data provided courtesy of Prof. H. Arenhövel.
- [38] G. Küster and H. Arenhövel, Mainz preprint MKPH-T-97-9 (March 1997), archive: nucl-th/9703036.
- [39] M.B. Barbaro, A. De Pace, T.W. Donnelly, A. Molinari Nucl. Phys. **A598**, 503 (1996).
- [40] R.L. Jaffe, Phys. Lett. **229B**, 275 (1989). M.J. Musolf and M. Burkhardt, Z. Phys. **C61**, 433 (1994). H. Forkel, M. Nielsen, X. Jin and T.D. Cohen, Phys. Rev. C **50**, 3108, (1994). M.J. Musolf, H.W. Hammer and D. Drechsel, archive: hep-ph/9610402.

APPENDIX A:

Here we present some details of the calculation of the hadronic tensor in RPWIA. After defining projected vectors

$$\begin{aligned}\mathcal{D}^\mu &\equiv r^\mu - d^\nu \frac{(d \cdot r)}{M_d^2} \\ N^\mu &\equiv n^\mu - d^\nu \frac{(d \cdot n)}{M_d^2},\end{aligned}\quad (\text{A1})$$

a straightforward calculation gives for the scalar term β in Eq. (9)

$$\begin{aligned}\beta &= 3mA^2 + \frac{B^2}{m} \mathcal{D}^2 - 2 \frac{AB}{m} (\mathcal{D} \cdot n) \\ &+ AF \left[3m - 3 \frac{(k \cdot n)}{m} + 2 \frac{(k \cdot N)}{m} \right] \\ &+ \frac{BG}{m} \mathcal{D}^2 \left[1 + \frac{(k \cdot n)}{m^2} \right] \\ &- \frac{AG + BF}{m} [(k \cdot \mathcal{D}) + (n \cdot \mathcal{D})]\end{aligned}$$

$$\begin{aligned}&+ \frac{G^2}{4m^3} \mathcal{D}^2 [(m^2 + k^2) + 2(k \cdot n)] \\ &+ \frac{F^2}{4m} [4(k \cdot N) - 6(k \cdot n) + 3(m^2 + k^2)] \\ &+ \frac{FG}{4m^3} [-2(m^2 + k^2)(\mathcal{D} \cdot n) - 4m^2(k \cdot \mathcal{D})] \quad , \quad (\text{A2})\end{aligned}$$

and for the vector term

$$\begin{aligned}\mathcal{P}^\mu &= A^2 [3n^\mu - 2N^\mu] - \frac{B^2 \mathcal{D}^2}{m^2} n^\mu + 2AB \mathcal{D}^\mu \\ &+ AF [3n^\mu - 2N^\mu - 3k^\mu] \\ &- \frac{BG}{m^2} \mathcal{D}^2 [k^\mu + n^\mu] \\ &+ \frac{AG + BF}{m^2} [m^2 \mathcal{D}^\mu + (n \cdot \mathcal{D}) k^\mu] \\ &+ \frac{AG - BF}{m^2} [(k \cdot n) \mathcal{D}^\mu - (k \cdot \mathcal{D}) n^\mu] \\ &+ \frac{G^2 \mathcal{D}^2}{4m^4} [(k^2 - m^2) n^\mu - 2 [(k \cdot n) + m^2] k^\mu] \\ &+ \frac{F^2}{4m^2} [[6(k \cdot n) - 4(k \cdot N) - 6m^2] k^\nu \\ &\quad + (k^2 - m^2) [2N^\nu - 3n^\nu]] \\ &+ \frac{FG}{4m^3} [4m(\mathcal{D} \cdot n) k^\mu + 4m(k \cdot \mathcal{D}) k^\mu \\ &\quad + 2m(m^2 - k^2) \mathcal{D}^\mu] \quad . \quad (\text{A3})\end{aligned}$$

Using the $\tilde{\Gamma}_2^\mu$ vertices of Eq. (50) and Eq. (14), the cc2 interference hadronic tensor [cf. Eq. (48)] reads

$$\begin{aligned}Z \tilde{H}_{cc2}^{\mu\nu} &= \tilde{F}_1 F_1 [S^\mu p^\nu + S^\nu p^\mu + g^{\mu\nu} (mT - (S \cdot p))] \\ &+ \frac{\tilde{F}_1 F_2}{2m} [g^{\mu\nu} (T(p \cdot q) - m(S \cdot q)) + q^\mu (mS^\nu - Tp^\nu)] \\ &+ \frac{\tilde{F}_2 F_1}{2m} [g^{\mu\nu} (T(p \cdot q) - m(S \cdot q)) + q^\nu (mS^\mu - Tp^\mu)] \\ &+ \frac{\tilde{F}_2 F_2}{4m^2} [g^{\mu\nu} [q^2(S \cdot p) + mTq^2 - 2(S \cdot q)(p \cdot q)] \\ &\quad - q^\mu q^\nu [(S \cdot p) + mT] + (p \cdot q) (S^\mu q^\nu + S^\nu q^\mu) \\ &\quad + (S \cdot q) (p^\mu q^\nu + p^\nu q^\mu) - q^2 (S^\mu p^\nu + S^\nu p^\mu)] \\ &+ i \tilde{G}_A F_1 \epsilon^{\mu\nu ab} S_a p_b + i \frac{\tilde{G}_A F_2}{2m} \epsilon^{\mu\nu ab} q_b (mS_a + Tp_a) \quad , \quad (\text{A4})\end{aligned}$$

with $Z = 3(k^2 - m^2)^2/4$. Analogously, for cc1

$$\begin{aligned}Z \tilde{H}_{cc1}^{\mu\nu} &= \tilde{G}_M G_M [S^\mu p^\nu + S^\nu p^\mu + g^{\mu\nu} (mT - (S \cdot p))] \\ &- \frac{\tilde{F}_2 G_M}{2m} (\bar{k} + p)^\mu (mS^\nu + Tp^\nu) \\ &- \frac{\tilde{G}_M F_2}{2m} (\bar{k} + p)^\nu (mS^\mu + Tp^\mu) \\ &+ \frac{\tilde{F}_2 F_2}{4m^2} (\bar{k} + p)^\mu (\bar{k} + p)^\nu (mT + (S \cdot p)) \\ &+ i \tilde{G}_A G_M \epsilon^{\mu\nu ab} S_a p_b \quad . \quad (\text{A5})\end{aligned}$$

The other tensors used in this work can be mapped to Eq. (A4) and Eq. (A5)

- for the electromagnetic hadronic tensors, $\tilde{F}_{1,2} \rightarrow F_{1,2}, \tilde{G}_A \rightarrow 0$.
- for the corresponding FPWIA tensors of Eq. (15),

$$\begin{pmatrix} S^\mu \\ T \end{pmatrix} \rightarrow Z \begin{pmatrix} \bar{k}^\mu \\ m \end{pmatrix}. \quad (\text{A6})$$

The cc1 [Eq. (A5)] and cc2 [Eq. (A4)] forms agree in the ‘‘on-shell’’ limit, consisting of (I) Eq. (A6), and (I) letting $q^\mu \rightarrow \bar{q}^\mu$, where $\bar{q}^\mu \equiv p^\mu - \bar{k}^\mu$. For example, under Eq. (A6) the $\tilde{F}_1 F_2$ terms in Eq. (A4) and Eq. (A5) become

$$\begin{aligned} \text{cc2} &\rightarrow \sim [g^{\mu\nu}(\bar{q}\cdot q) - q^\mu \bar{q}^\nu] \\ \text{cc1} &\rightarrow \sim [2g^{\mu\nu}(m^2 - \bar{k}\cdot p) - (\bar{k} - p)^\mu (\bar{k} - p)^\nu] \\ &= [g^{\mu\nu}(\bar{q}\cdot \bar{q}) - q^\mu \bar{q}^\nu], \end{aligned} \quad (\text{A7})$$

which coincide under $q^\mu \rightarrow \bar{q}^\mu$.

APPENDIX B:

Here we evaluate the $(+, -)$ and $(-, +)$ contributions to Eq. (23), using the relevant spectral function [cf. Eq. (28)]. Notice that we have chosen to define ξ^μ in terms of the positive energy spinors $u(\mathbf{k}, s)$. Thus, $k_+\cdot\xi = 0$ but $k_-\cdot\xi = n\cdot\xi = 2\bar{E}_k\xi^0 \neq 0$. The spin sums are evaluated using $\sum_s \xi_{s,s}^\mu = 0$ and $\sum_s \sum_r \xi_{s,r}^\mu \xi_{r,s}^\nu = 2(-g^{\mu\nu} + \bar{k}^\mu \bar{k}^\nu / m^2)$. Since ρ_{+-} is linear in ξ_μ and because of the first of these properties, there is no contribution in Eq. (25) from the $\delta_{s,r}$ part of the projector in Eq. (26). Thus, effectively,

$$\begin{aligned} \chi_+^s \bar{\chi}_-^r + \chi_-^s \bar{\chi}_+^r &\rightarrow \frac{\bar{k} + m}{4m} \gamma_5 \xi^* \gamma_5 \gamma^0 + \gamma_5 \gamma^0 \frac{\bar{k} + m}{4m} \gamma_5 \xi^* \\ &= (\bar{E}_k \xi^* - (\bar{k} + m)\xi^{*0}) / 2m, \end{aligned} \quad (\text{B1})$$

with $\xi \equiv \xi_{s,r} = \xi_{r,s}^*$. Therefore, from Eqs. (25) and (27)

$$\begin{aligned} \sum_{\text{spins}} \rho_{+-;rs} (\chi_+^s \bar{\chi}_-^r + \chi_-^s \bar{\chi}_+^r) &= \frac{c}{2m} \sum_{\text{spins}} \left\{ [\bar{k}\cdot\mathcal{P} + m\beta] \xi^0 \right. \\ &\times [\xi^{*0}(\bar{k} + m) - \xi^* \bar{E}_k] + \bar{E}_k (\xi\cdot\mathcal{P}) [\bar{E}_k \xi^* - (\bar{k} + m)\xi^{*0}] \left. \right\} \\ &= -\frac{c}{m^3} \left[(\bar{k}\cdot\mathcal{P} + m\beta) [(\bar{k} + m)(m^2 - \bar{E}_k^2) \right. \\ &\quad - \bar{E}_k (m^2 \gamma^0 - \bar{E}_k \bar{k})] + \bar{E}_k^2 [m^2 \mathcal{P} - \bar{k} \bar{k}\cdot\mathcal{P}] \\ &\quad \left. - \bar{E}_k^2 (\bar{k} + m) [m^2 \mathcal{P}^0 - \bar{k}\cdot\mathcal{P}] \right] \\ &= -\frac{c}{2m} \left([-n\cdot\mathcal{P} + m\beta] (\bar{k} + m) - [\bar{k}\cdot\mathcal{P} + m\beta] (\not{n} - m) \right. \\ &\quad \left. + [m^2 + (\bar{k}\cdot n)] (\mathcal{P} - \beta) \right), \end{aligned} \quad (\text{B2})$$

where we have set $c = f_+ f_- / 12\pi^3 M_d (k^2 - m^2)^2$, and used $\bar{E}_k \gamma^0 = (\bar{k} + \not{n})/2$, $\bar{E}_k \mathcal{P}^0 = (\bar{k}\cdot\mathcal{P} + n\cdot\mathcal{P})/2$, and $\bar{E}_k^2 = (m^2 + \bar{k}\cdot n)/2$. We finally obtain

$$\begin{aligned} &\sum_{\text{spins}} (\rho_{+-;rs} \mathcal{H}_{+-;rs}^{\mu\nu} + \rho_{-+;rs} \mathcal{H}_{-+;rs}^{\mu\nu}) \\ &= \frac{f_+}{f_-} \rho_{--} \mathcal{H}_{++}^{\mu\nu} + \frac{f_-}{f_+} \rho_{++} \mathcal{H}_{--}^{\mu\nu} \\ &\quad - \frac{f_+ f_- [m^2 + (\bar{k}\cdot n)]}{12\pi^3 M_d (k^2 - m^2)^2} \text{Tr} \left\{ \frac{\mathcal{P} - \beta}{2m} \bar{\Gamma}^\mu \frac{\not{n} + m}{2m} \Gamma^\nu \right\}. \end{aligned} \quad (\text{B3})$$

Let us compare Eq. (B3) with Eq. (17). The first two ‘‘mixed’’ terms in Eq. (B3) correspond to the $(+, -)$ contribution to the first term in the RHS of Eq. (17), while the last term, which spoils factorization, derives from the second term in the RHS of Eq. (17), as anticipated in Eq. (31).